Moment Closure for Local Control Models of Calcium-Induced Calcium Release in Cardiac Myocytes

George S. B. Williams,* Marco A. Huertas,* Eric A. Sobie,† M. Saleet Jafri,‡ and Gregory D. Smith*§
*Department of Applied Science, College of William and Mary, Williamsburg, Virginia; †Department of Bioinformatics and Computational Biology, George Mason University, Manassas, Virginia; ‡Department of Pharmacology and Systems Therapeutics, Mount Sinai School of Medicine, New York, New York; and §Mathematical Biosciences Institute, The Ohio State University, Columbus, Ohio

ABSTRACT In prior work, we introduced a probability density approach to modeling local control of Ca^{2+}-induced Ca^{2+} release in cardiac myocytes, where we derived coupled advection-reaction equations for the time-dependent bivariate probability density of subsarcolemmal subspace and junctional sarcoplasmic reticulum (SR) $[Ca^{2+}]$ conditioned on Ca^{2+} release unit (CaRU) state. When coupled to ordinary differential equations (ODEs) for the bulk myoplasmic and network SR $[Ca^{2+}]$, a realistic but minimal model of cardiac excitation-contraction coupling was produced that avoids the computationally demanding task of resolving spatial aspects of global Ca^{2+} signaling, while accurately representing heterogeneous local Ca^{2+} signals in a population of diadic subspaces and junctional SR depletion domains. Here we introduce a computationally efficient method for simulating such whole cell models when the dynamics of subspace $[Ca^{2+}]$ are much faster than those of junctional SR $[Ca^{2+}]$. The method begins with the derivation of a system of ODEs describing the time-evolution of the moments of the univariate probability density functions for junctional SR $[Ca^{2+}]$ jointly distributed with CaRU state. This open system of ODEs is then closed using an algebraic relationship that expresses the third moment of junctional SR $[Ca^{2+}]$ in terms of the first and second moments. In simulated voltage-clamp protocols using 12-state CaRUs that respond to the dynamics of both subspace and junctional SR $[Ca^{2+}]$, this moment-closure approach to simulating local control of excitation-contraction coupling produces high-gain Ca^{2+} release that is graded with changes in membrane potential, a phenomenon not exhibited by common pool models. Benchmark simulations indicate that the moment-closure approach is nearly 10,000-times more computationally efficient than corresponding Monte Carlo simulations while leading to nearly identical results. We conclude by applying the moment-closure approach to study the restitution of Ca^{2+}-induced Ca^{2+} release during simulated two-pulse voltage-clamp protocols.

INTRODUCTION

The key step linking electrical excitation to contraction in cardiac myocytes is Ca^{2+}-induced Ca^{2+} release (CICR), in which Ca^{2+} current flowing across the cell membrane triggers the release of additional Ca^{2+} from the sarcoplasmic reticulum (SR). In ventricular cells, CICR occurs as a set of discrete microscopic events known as Ca^{2+} sparks (1), with each spark triggered by local, rather than cell-wide, increases in myoplasmic $[Ca^{2+}]$. As a consequence of this local-control mechanism of CICR, the cellular SR Ca^{2+} release flux is not a function of a single quantity, such as spatially averaged intracellular $[Ca^{2+}]$, but instead depends on thousands of different local Ca^{2+} concentrations, each of which can fluctuate with stochastic openings and closings of nearby Ca^{2+} channels in the sarcolemmal and SR membranes. The picture is further complicated by the fact that dynamic changes in local SR $[Ca^{2+}]$, which are also spatially heterogeneous, are thought to influence the gating of SR Ca^{2+} release channels known as ryanodine receptors (RyRs).

Computational models have been developed in which SR Ca^{2+} release depends directly on the average myoplasmic $[Ca^{2+}]$ (2–4). These so-called common-pool models (5) display SR Ca^{2+} release that occurs in an all-or-none fashion, contrary to experiments showing that release is smoothly graded with changes in Ca^{2+} influx (6–8). On the other hand, several published models achieve graded Ca^{2+} release using nonmechanistic formulations, such as having SR Ca^{2+} release depend explicitly on Ca^{2+} currents rather than on local $[Ca^{2+}]$ (9–13).

Models of EC coupling are able to reproduce graded Ca^{2+} release mechanistically by simulating the stochastic gating of channels in Ca^{2+} release sites using Monte Carlo methods. In these approaches, one or more L-type Ca^{2+} channels interact with a cluster of RyRs through changes in $[Ca^{2+}]$ in a small diadic subspace between the sarcolemmal and SR membranes. These models also generally consider local changes in junctional SR $[Ca^{2+}]$, because these changes are thought to be important for Ca^{2+} spark termination and refractoriness (14–16). Realistic cellular SR Ca^{2+} release can be simulated by computing the stochastic triggering of sparks from hundreds to thousands of such Ca^{2+} release units (CaRUs) (5,15–17). However, Monte Carlo simulations of local control of EC coupling can be computationally demanding, making it difficult to augment these models with representations of the ionic currents responsible for action potentials, and impractical to use this approach for simulations of phenomena occurring over the course of many heartbeats.

We recently demonstrated that an alternative probability-density approach can be used to simulate graded, locally controlled SR Ca^{2+} release mechanistically (18). In this prior

Submitted November 18, 2007, and accepted for publication April 18, 2008.

George S. B. Williams and Marco A. Huertas contributed equally to this work.

Address reprint requests to Gregory D. Smith, E-mail: greg@as.wm.edu.

Editor: David A. Eisner.

0006-3495/08/08/1689/15 $2.00

doi: 10.1529/biophysj.107.125948

work, coupled advection-reaction equations were derived relating the time-dependent probability density of subsarcolemmal subspace and junctional SR $[Ca^{2+}]$ conditioned on CaRU state. By numerically solving these equations using a high-resolution finite difference scheme and coupling the resulting probability densities to ordinary differential equations (ODEs) for the bulk myoplasmic and sarcoplasmic reticulum $[Ca^{2+}]$, a realistic but minimal model of cardiac excitation-contraction coupling was produced. This new approach to modeling local control of EC coupling is often computationally more efficient than Monte Carlo simulation, particularly if the dynamics of subspace $[Ca^{2+}]$ are much faster that those of junctional SR $[Ca^{2+}]$, allowing the bivariate probability density functions for subspace and junctional SR $[Ca^{2+}]$ to be replaced with univariate densities for junctional SR $[Ca^{2+}]$. However, the probability density approach can lose its computational advantage when the number of states in the CaRU model is large or the dynamics of local $[Ca^{2+}]$ are such that numerical stability requires a refined mesh for solving the advection-reaction equations.

We therefore aimed to develop methods for improving upon the probability-density approach, and in this study, we describe a moment-closure technique that leads to significant computational advantages. After briefly reviewing the Monte Carlo and probability density approaches to modeling local control of EC coupling in cardiac myocytes, the new methodology begins with a derivation of a system of ODEs describing the time-evolution of the moments of the univariate probability density functions for junctional SR $[Ca^{2+}]$ jointly distributed with CaRU state. This open system of ODEs is then closed using an algebraic relationship that expresses the third moment of junctional SR $[Ca^{2+}]$ in terms of the first and second moments. In this manner, the partial differential equations describing the univariate probability densities of junctional SR $[Ca^{2+}]$ jointly distributed with CaRU state are replaced with ODEs describing the time-evolution of the moments of these distributions. In simulated voltage-clamp protocols using 12-state CaRUs that respond to the dynamics of both subspace and junctional SR $[Ca^{2+}]$, this moment-closure approach to simulating local control of EC coupling produces high-gain Ca^{2+} release that is graded with changes in membrane potential, a phenomenon not exhibited by common pool models. Benchmark simulations indicate that this moment-closure technique for local control models of CICR in cardiac myocytes is nearly 10,000-times more computationally efficient than corresponding Monte Carlo simulations, while leading to nearly identical results. We conclude by applying the moment-closure approach to study the restitution of Ca^{2+}-induced Ca^{2+} release during simulated two-pulse voltage-clamp protocols.

MODEL FORMULATION

The focus of this article is a moment-closure technique to modeling local control of CICR in cardiac myocytes. The whole cell model of EC coupling that will be used to demonstrate the method closely follows our prior work in which we presented traditional Monte Carlo simulations of graded, locally controlled SR Ca^{2+} release to validate a novel probability density approach that represents the distribution of diadic subspace and junctional SR Ca^{2+} concentrations with a system of partial differential equations (18). Below we briefly review the Monte Carlo and probability density formulations, emphasizing minor adjustments that were required to implement the moment-closure technique. The Results section begins with the derivation of the moment-closure equations and follows with the validation and benchmarking of the moment-closure technique for local control models of CICR in cardiac myocytes by comparison to Monte Carlo simulation.

Monte Carlo formulation

The Monte Carlo model of local control of CICR in cardiac myocytes describes the dynamics of bulk myoplasmic $[Ca^{2+}]$, network SR $[Ca^{2+}]$, N diadic subspace Ca^{2+} concentrations, and N junctional SR domain Ca^{2+} concentrations through a system of ODEs. These are coupled to N Markov chains representing the stochastic gating of each CaRU that consists of one L-type Ca^{2+} channel (DHPR) and one RyR megachannel coupled through the local diadic subspace (c_{ds}) $[Ca^{2+}]$. While a complete description of CICR would include stochastic gating of roughly $N = 10{,}000$ CaRUs, each containing multiple L-type Ca^{2+} channels (1–10) (19) and RyRs (30–300) (20), Monte Carlo simulations of EC coupling focusing on local control have often used Markov models of reduced complexity (5,16,21). This level of resolution will suffice to introduce the moment-closure technique.

Concentration balance equations

The Monte Carlo model consists of $N+2$ ODEs representing the time-evolution of $[Ca^{2+}]$ in the bulk myoplasm (c_{myo}), network SR (c_{nsr}), and N junctional SRs (c_{jsr}^{n}) compartments. Consistent with Fig. 1, the concentration balance equations for these compartments are

$$\frac{dc_{myo}}{dt} = J_{leak} + J_{efflux}^{T} - J_{ncx} - J_{serca} + J_{in}, \quad (1)$$

$$\frac{dc_{nsr}}{dt} = \frac{1}{\lambda_{nsr}}(J_{serca} - J_{refill}^{T} - J_{leak}), \quad (2)$$

$$\frac{dc_{jsr}^{n}}{dt} = \frac{1}{\lambda_{jsr}}(J_{refill}^{n} - J_{ryr}^{n}), \quad (3)$$

where $1 \le n \le N$ and λ_{nsr} and λ_{jsr} are volume fractions (see the Appendix). The flux through the RyR megachannel associated with the n^{th} CaRU (J_{ryr}^{n}) is given by

$$J_{ryr}^{n} = \gamma_{ryr}^{n}\frac{v_{ryr}^{T}}{N}(c_{jsr}^{n} - \bar{c}_{ds}^{n}), \quad (4)$$

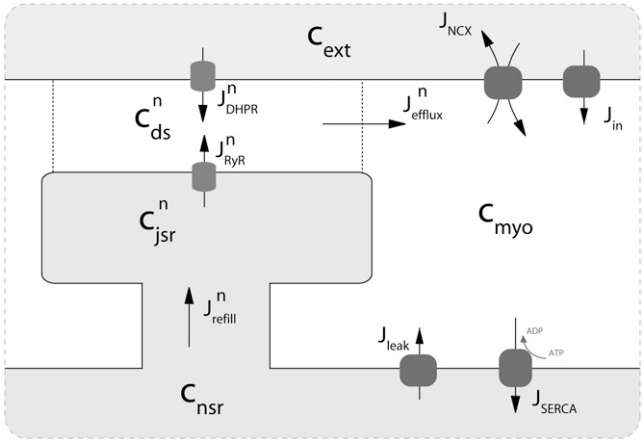

FIGURE 1 Diagram of model components and fluxes. Each Ca^{2+} release unit consists of two restricted compartments (the diadic subspace and junctional SR with $[Ca^{2+}]$ denoted by c_{ds} and c_{jsr}, respectively), a two-state L-type Ca^{2+} channel (DHPR), and a six-state Ca^{2+} release site. The t-tubular $[Ca^{2+}]$ is denoted by c_{ext} and the fluxes $J^n_{dhpr}, J^n_{ryr}, J^n_{efflux}, J^n_{refill}, J_{in}, J_{ncx}, J_{serca}$, and J_{leak} are described in the text and the Appendix.

where γ^n_{ryr} is a stochastic variable that takes the value 1 or 0 depending on whether the n^{th} RyR megachannel is open or closed, and $\bar{c}^n_{ds}$ is the associated diadic subspace concentration defined below (Eq. 9). Similarly, diffusion from the network SR to each junctional SR compartment is given by

$$J^n_{refill} = \frac{v^T_{refill}}{N}(c_{nsr} - c^n_{jsr}). \tag{5}$$

The total refill flux occurring in Eq. 2 includes the contribution from each CaRU and is given by

$$J^T_{refill} = \sum_{n=1}^{N} J^n_{refill}, \tag{6}$$

while the total flux out of the N diadic subspaces is given by

$$J^T_{ef\,flux} = \sum_{n=1}^{N} J^n_{ef\,flux} = \sum_{n=1}^{N} \frac{v^T_{ef\,flux}}{N}(\bar{c}^n_{ds} - c_{myo}). \tag{7}$$

The remaining four fluxes that appear in Eqs. 1–3 and Fig. 1 include J^n_{dhpr} (influx into the diadic subspaces via L-type Ca^{2+} channels which are functions of the random variable γ^n_{dhpr}), J_{in} (background Ca^{2+} influx), J_{ncx} (Na^+-Ca^{2+} exchange), J_{serca} (SR Ca^{2+}-ATPases), and J_{leak} (the network SR leak). The functional form of these four fluxes can be found in the Appendix.

Diadic subspace Ca^{2+} concentration

Note that a concentration balance equation is not included for diadic subspace $[Ca^{2+}]$, because in our previous study we observed that model parameters lead to rapid equilibrium of the diadic subspace $[Ca^{2+}]$ with the $[Ca^{2+}]$ in the junctional SR and bulk myoplasm (18). Thus, in each diadic subspace we assume a $[Ca^{2+}]$ ($\bar{c}^n_{ds}$) that balances the fluxes in and out of that compartment,

$$0 = \frac{1}{\lambda_{ds}}(J^n_{dhpr} + J^n_{ryr} - J^n_{efflux}); \tag{8}$$

that is,

$$\bar{c}^n_{ds} = \bar{c}^n_{ds,0} + \bar{c}^n_{ds,1}\, c_{jsr} \tag{9}$$

where $1 \le n \le N$ and

$$\bar{c}^n_{ds,0} = \frac{\gamma^n_{dhpr} J^0_{dhpr} + v_{ef\,flux} c_{myo}}{\gamma^n_{ryr} v_{ryr} + v_{ef\,flux} - \gamma^n_{dhpr} J^1_{dhpr}}, \tag{10}$$

$$\bar{c}^n_{ds,1} = \frac{\gamma^n_{ryr} v_{ryr}}{\gamma^n_{ryr} v_{ryr} + v_{efflux} - \gamma^n_{dhpr} J^1_{dhpr}}. \tag{11}$$

In these expressions, the quantities γ^n_{dhpr} and γ^n_{ryr} indicate whether the channel is open or closed, and $v_{ryr} = v^T_{ryr}/N$, $v_{efflux} = v^T_{efflux}/N$, and J^0_{dhpr} and J^1_{dhpr} are functions of plasma membrane voltage defined by

$$J^n_{dhpr} = \gamma^n_{dhpr}(J^0_{dhpr} + \bar{c}^n_{ds} J^1_{dhpr}), \tag{12}$$

where the L-type Ca^{2+} channel flux, J^n_{dhpr} is given by Eq. 56 (see the Appendix).

Twelve-state CaRU model

The RyR model used here is similar to the two-state minimal model of an RyR megachannel used in prior work (18). Consistent with several studies indicating that the gating of the RyR cluster associated with each CaRU is essentially all-or-none (5,15,16), the two-state RyR megachannel model used in Williams et al. (18) included transition rates that were nonlinear functions of diadic subspace (c_{ds}) and junctional SR (c_{jsr}) $[Ca^{2+}]$, thereby allowing for Ca^{2+}-dependent activation of RyR gating as well as spark termination facilitated by localized depletion of junctional SR $[Ca^{2+}]$. Because the moment-closure approach is most easily presented when all Ca^{2+}-mediated transitions in the CaRU model are bimolecular association reactions, the six-state RyR megachannel model used here employs sequential binding of diadic subspace Ca^{2+} ions to achieve highly cooperative Ca^{2+}-dependent opening of the RyR megachannel. Similarly, an explicit junctional SR Ca^{2+}-dependent transition is included so that depletion of luminal Ca^{2+} decreases the open probability of the megachannel,

$$\mathcal{C}_1 \underset{\beta^3 k^-_{ryr}}{\overset{4k^+_{ryr}c_{ds}}{\rightleftharpoons}} \mathcal{C}_2 \underset{2\beta^2 k^-_{ryr}}{\overset{3\alpha k^+_{ryr}c_{ds}}{\rightleftharpoons}} \mathcal{C}_3 \underset{3\beta k^-_{ryr}}{\overset{2\alpha^2 k^+_{ryr}c_{ds}}{\rightleftharpoons}} \mathcal{C}_4 \underset{4k^-_{ryr}}{\overset{\alpha^3 k^+_{ryr}c_{ds}}{\rightleftharpoons}} \mathcal{C}_5 \underset{k^-_{ryr,*}}{\overset{k^+_{ryr,*}c_{jsr}}{\rightleftharpoons}} \mathcal{O}. \tag{13}$$

Parameters were chosen (see Table 3) so that the behavior of this minimal six-state RyR megachannel model approximated the above-mentioned two-state model.

As in prior work (18), we use a two-state model of the L-type Ca^{2+} channel (DHPR),

$$\mathcal{C} \underset{k^-_{\mathrm{dhpr}}}{\overset{k^+_{\mathrm{dhpr}}(V)}{\rightleftharpoons}} \mathcal{O}, \tag{14}$$

where $\mathcal{C}$ and $\mathcal{O}$ represent closed and open states, k^+_{dhpr} is the voltage-dependent activation rate (10) given by

$$k^+_{\mathrm{dhpr}} = \bar{k}^+_{\mathrm{dhpr}} \frac{e^{(V-V^{\theta}_{\mathrm{dhpr}})/\sigma_{\mathrm{dhpr}}}}{1+e^{(V-V^{\theta}_{\mathrm{dhpr}})/\sigma_{\mathrm{dhpr}}}}, \tag{15}$$

and k^-_{dhpr} is the constant deactivation rate that sets the mean open time (0.2 ms) and maximum open probability (0.1) of the channel. Although this two-state DHPR model ignores voltage- and Ca^{2+}-dependent inactivation of L-type Ca^{2+} channels, these processes do not significantly influence the triggering of CICR during the whole-cell voltage clamp protocols that are used in this article to validate the moment-closure technique.

Combining the six-state RyR megachannel model with the two-state L-type channel model yields a 12-state CaRU model that takes the form

$$\begin{array}{ccccccccccc} \mathcal{CC}_1 & \rightleftharpoons & \mathcal{CC}_2 & \rightleftharpoons & \mathcal{CC}_3 & \rightleftharpoons & \mathcal{CC}_4 & \rightleftharpoons & \mathcal{CC}_5 & \rightleftharpoons & \mathcal{CO} \\ \uparrow\downarrow & & \uparrow\downarrow & & \uparrow\downarrow & & \uparrow\downarrow & & \uparrow\downarrow & & \uparrow\downarrow \\ \mathcal{OC}_1 & \rightleftharpoons & \mathcal{OC}_2 & \rightleftharpoons & \mathcal{OC}_3 & \rightleftharpoons & \mathcal{OC}_4 & \rightleftharpoons & \mathcal{OC}_5 & \rightleftharpoons & \mathcal{OO} \end{array}, \tag{16}$$

where horizontal and vertical transitions are governed by Eqs. 13 and 14, respectively, and the first character ($\mathcal{C}$ or $\mathcal{O}$) indicates the state of the DHPR while the second character ($\mathcal{C}_1, \mathcal{C}_2, \mathcal{C}_3, \mathcal{C}_4, \mathcal{C}_5$, or $\mathcal{O}$) refers to the state of the RyR megachannel.

Note that the 12×12 infinitesimal generator matrix (sometimes called the Q-matrix) that collects the rate constants of the CaRU model (Eq. 16) can be written compactly in the form

$$Q = K_{\phi}(V) + c_{\mathrm{ds}} K_{\mathrm{ds}} + c_{\mathrm{jsr}} K_{\mathrm{jsr}}, \tag{17}$$

where the elements of $K_{\phi}(V)$ are the Ca^{2+}-independent transitions (both voltage-dependent and voltage-independent with units of time^{-1}), and the elements of K_{ds} and K_{jsr} are the association rate constants for the transitions mediated by diadic subspace (c_{ds}) and junctional SR (c_{jsr}) [Ca^{2+}], respectively (with units of concentration^{-1} time^{-1}). Although noncooperative binding of Ca^{2+} is not a formal requirement for the application of the moment-closure technique, for simplicity we will assume the CaRU model is written in the form of Eq. 17.

Univariate probability density model

The moment-closure technique begins with the equations for a univariate probability density model of local control of Ca^{2+}-induced Ca^{2+} release in cardiac myocytes (18). We write $\rho^{\mathrm{i}}(c_{\mathrm{jsr}}, t)$ to denote probability density functions for the distribution of [Ca^{2+}] in a large number of junctional SR compartments jointly distributed with CaRU state, that is,

$$\rho^{\mathrm{i}}(c_{\mathrm{jsr}}, t)\, dc_{\mathrm{jsr}} = \Pr\{c_{\mathrm{jsr}} < \tilde{c}_{\mathrm{jsr}}(t) < c_{\mathrm{jsr}} + dc_{\mathrm{jsr}} \quad \text{and} \quad \tilde{S}(t) = i\}, \tag{18}$$

where i is an index over CaRU state, and the tilde in $\tilde{c}_{\mathrm{jsr}}$ and $\tilde{S}$ indicate random quantities. For these densities to be consistent with the dynamics of the Monte Carlo model of cardiac EC coupling as $N \to \infty$, they must satisfy a system of advection-reaction equations of the form (18,22,23)

$$\frac{\partial \rho^{\mathrm{i}}}{\partial t} = -\frac{\partial}{\partial c_{\mathrm{jsr}}}[f^{\mathrm{i}}_{\mathrm{jsr}}\, \rho^{\mathrm{i}}] + [\rho Q]^{\mathrm{i}}, \tag{19}$$

where $1 \le i \le M, M = 12$ is the number of states in the CaRU model, Q is the $M \times M$ generator matrix (Eq. 17), the row-vector $\rho(c_{\mathrm{jsr}}, t) = (\rho^1, \rho^2, \cdots, \rho^{\mathrm{M}})$ collects the time-dependent probability densities for the junctional SR [Ca^{2+}] jointly distributed with CaRU state (Eq. 18), and $[\rho Q]^{\mathrm{i}}$ is the i^{th} element of the vector-matrix product ρQ.

Note that the factor $f^{\mathrm{i}}_{\mathrm{jsr}}(c_{\mathrm{jsr}})$ in Eq. 19 describes the deterministic aspect of the time-evolution of c_{jsr} when the CaRU is in state i. That is, consistent with Eq. 3 we have

$$\begin{aligned} f^{\mathrm{i}}_{\mathrm{jsr}} &= \frac{1}{\lambda^{\mathrm{T}}_{\mathrm{jsr}}}(J^{\mathrm{T}}_{\mathrm{refill}} - \gamma^{\mathrm{i}}_{\mathrm{ryr}} J^{\mathrm{T}}_{\mathrm{ryr}}) \\ &= \frac{1}{\lambda^{\mathrm{T}}_{\mathrm{jsr}}}\Big(v^{\mathrm{T}}_{\mathrm{refill}}\big[c_{\mathrm{nsr}} - c_{\mathrm{jsr}}\big] - \gamma^{\mathrm{i}}_{\mathrm{ryr}} v^{\mathrm{T}}_{\mathrm{ryr}}\big[c_{\mathrm{jsr}} - \bar{c}^{\mathrm{i}}_{\mathrm{ds}}\big]\Big), \end{aligned} \tag{20}$$

where $1 \le i \le M$ and $\bar{c}^{\mathrm{i}}_{\mathrm{ds}}$ is a function of CaRU state, the local junctional SR [Ca^{2+}], and the bulk myoplasmic [Ca^{2+}] analogous to Eqs. 9–11,

$$\bar{c}^{\mathrm{i}}_{\mathrm{ds}} = \bar{c}^{\mathrm{i}}_{\mathrm{ds},0} + \bar{c}^{\mathrm{i}}_{\mathrm{ds},1}\, c_{\mathrm{jsr}}, \tag{21}$$

where

$$\bar{c}^{\mathrm{i}}_{\mathrm{ds},0} = \frac{\gamma^{\mathrm{i}}_{\mathrm{dhpr}} J^{\mathrm{T},0}_{\mathrm{dhpr}} + v^{\mathrm{T}}_{\mathrm{ef\,flux}} c_{\mathrm{myo}}}{\gamma^{\mathrm{i}}_{\mathrm{ryr}} v^{\mathrm{T}}_{\mathrm{ryr}} + v^{\mathrm{T}}_{\mathrm{ef\,flux}} - \gamma^{\mathrm{i}}_{\mathrm{dhpr}} J^{\mathrm{T},1}_{\mathrm{dhpr}}}, \tag{22}$$

$$\bar{c}^{\mathrm{i}}_{\mathrm{ds},1} = \frac{\gamma^{\mathrm{i}}_{\mathrm{ryr}} v^{\mathrm{T}}_{\mathrm{ryr}}}{\gamma^{\mathrm{i}}_{\mathrm{ryr}} v^{\mathrm{T}}_{\mathrm{ryr}} + v^{\mathrm{T}}_{\mathrm{ef\,flux}} - \gamma^{\mathrm{i}}_{\mathrm{dhpr}} J^{\mathrm{T},1}_{\mathrm{dhpr}}}. \tag{23}$$

In these expressions, the quantities $\gamma^{\mathrm{i}}_{\mathrm{dhpr}}$ and $\gamma^{\mathrm{i}}_{\mathrm{ryr}}$ take values of 0 or 1 depending on whether the respective component of the CaRU model is closed or open, and $J^{\mathrm{T},0}_{\mathrm{dhpr}}$ and $J^{\mathrm{T},1}_{\mathrm{dhpr}}$ are functions of plasma membrane voltage defined by

$$J^{\mathrm{T}}_{\mathrm{dhpr}} = \sum_{\mathrm{i}=1}^{\mathrm{M}} \gamma^{\mathrm{i}}_{\mathrm{dhpr}}(J^{\mathrm{T},0}_{\mathrm{dhpr}} + \bar{c}^{\mathrm{i}}_{\mathrm{ds}} J^{\mathrm{T},1}_{\mathrm{dhpr}}), \tag{24}$$

where J^{T}_{dhpr} is the total flux through the L-type Ca^{2+} channels (Eq. 58).

Conversely, the reaction terms ($[\rho Q]^{i}$) on the right-hand side of Eq. 19 correspond to the stochastic aspect of the CaRU dynamics (i.e., changes in probability due to the stochastic gating of the RyR megachannel and DHPRs). This term involves processes that may depend on the junctional SR [Ca^{2+}] directly (as in the transition $\mathcal{CC}_5 \rightarrow \mathcal{CO}$) or indirectly (as in the transition $\mathcal{CC}_4 \rightarrow \mathcal{CC}_5$), as well as terms dependent on the membrane voltage (such as the transition $\mathcal{CC}_1 \rightarrow \mathcal{OC}_1$). Using the decomposition of Q given by Eq. 17, one can see that $[\rho Q]^{i}$ is a function of V and c_{jsr} given by

$$[\rho Q]^{i} = \sum_{j=1}^{M} \rho^{j}\left[K_{\phi}^{j,i} + \bar{c}_{ds}^{j} K_{ds}^{j,i} + c_{jsr} K_{jsr}^{j,i}\right] = \sum_{j=1}^{M} \rho^{j}\left[K_{\phi}^{j,i} + \bar{c}_{ds,0}^{j} K_{ds}^{j,i} + c_{jsr}(\bar{c}_{ds,1}^{j} K_{ds}^{j,i} + K_{jsr}^{j,i})\right], \quad (25)$$

where $K_{\phi}(V)$ provides the voltage-dependence, the superscripts of $K_{\phi}^{j,i}$, $K_{ds}^{j,i}$, and $K_{jsr}^{j,i}$ indicate row and column indices of these matrices, $\rho^{i}(c_{jsr}, t)$ is the probability density for state j, and $\bar{c}_{ds,0}^{j}$ and $\bar{c}_{ds,1}^{j}$ are given by Eqs. 21–23.

The concentration balance equations governing the bulk myoplasmic (c_{myo}) and network SR (c_{nsr}) [Ca^{2+}] in the probability density formulation are identical to those used in the Monte Carlo approach (Eqs. 1–2), except that the fluxes J^{T}_{refill} and J^{T}_{efflux} are dependent on the densities (ρ^{i}_{jsr}); that is,

$$J^{T}_{refill} = \sum_{i=1}^{M} \int_{0}^{\infty} v^{T}_{refill}\left[c_{nsr} - c_{jsr}\right]\rho^{i}_{jsr}(c_{jsr}, t)dc_{jsr}, \quad (26)$$

$$J^{T}_{ef\,flux} = \sum_{i=1}^{M} \int_{0}^{\infty} v^{T}_{ef\,flux}\left[\bar{c}^{i}_{ds} - c_{myo}\right]\rho^{i}_{jsr}(c_{jsr}, t)dc_{jsr}, \quad (27)$$

where $\bar{c}^{i}_{ds}$ is a function of c_{jsr} (Eq. 21).

RESULTS

Moments of junctional SR [Ca^{2+}]

The application of the moment-closure technique to the local control model of Ca^{2+}-induced Ca^{2+} release (CICR) in cardiac myocytes presented above begins by writing the q^{th} moment of the univariate probability density function, $\rho^{i}(c_{jsr}, t)$, as

$$\mu^{i}_{q}(t) = \int (c_{jsr})^{q}\rho^{i}(c_{jsr}, t)dc_{jsr}, \quad (28)$$

where the nonnegative integer q indicates the moment degree in μ^{i}_{q} and is an exponent in $(c_{jsr})^{q}$. As defined in Eq. 18, $\rho^{i}(c_{jsr}, t)$ is the distribution of [Ca^{2+}] in a large number of junctional SR compartments jointly distributed with CaRU state. Thus, the zeroth moment μ^{i}_{0} corresponds to the probability—denoted as $\pi^{i}(t)$ in Williams et al. (18)—that a randomly sampled CaRU is in state i; that is,

$$\pi^{i}(t) = \mu^{i}_{0}(t) = \int \rho^{i}(c_{jsr}, t)dc_{jsr} = \Pr\{\tilde{S}(t) = i\},$$

where conservation of probability implies $\sum_{i}\pi^{i} = 1$. Because the joint probability densities do not individually integrate to unity, the first moment,

$$\mu^{i}_{1}(t) = \int c_{jsr}\,\rho^{i}(c_{jsr}, t)dc_{jsr}$$

is related to the expected value of the junctional SR [Ca^{2+}] conditioned on CaRU state through

$$E^{i}[\tilde{c}_{jsr}] = \frac{\mu^{i}_{1}}{\mu^{i}_{0}}, \quad (29)$$

while the conditional variance of the junctional SR [Ca^{2+}] is

$$Var^{i}[\tilde{c}_{jsr}] = \frac{\mu^{i}_{2}}{\mu^{i}_{0}} - \left(\frac{\mu^{i}_{1}}{\mu^{i}_{0}}\right)^{2}. \quad (30)$$

Expressing fluxes in terms of moments

Considering Eqs. 1 and 2 and Eqs. 26–27, one sees that the fluxes J^{T}_{efflux} and J^{T}_{refill} mediate the influence of the distribution of diadic subspace and junctional SR [Ca^{2+}] on the dynamics of the bulk myoplasmic [Ca^{2+}] (c_{myo}) and the network SR [Ca^{2+}] (c_{nsr}). Using the definition of the moments of junctional SR [Ca^{2+}] (Eq. 28), these fluxes become functions of the zeroth and first moments,

$$J^{T}_{refill} = \sum_{i=1}^{M} v^{T}_{refill}(c_{nsr}\mu^{i}_{0} - \mu^{i}_{1})$$

$$J^{T}_{ef\,flux} = \sum_{i=1}^{M} v^{T}_{ef\,flux}(\bar{c}^{i}_{ds,0}\,\mu^{i}_{0} + \bar{c}^{i}_{ds,1}\,\mu^{i}_{1} - c_{myo}\mu^{i}_{0}). \quad (31)$$

Similarly, the total flux through all the L-type Ca^{2+} channels (J^{T}_{dhpr}, Eq. 24) and the RyR Ca^{2+} channels (J^{T}_{ryr}) become

$$J^{T}_{dhpr} = \sum_{i=1}^{M} \gamma^{i}_{dhpr}\left[J^{0}_{dhpr}\mu^{i}_{0} + J^{1}_{dhpr}(\bar{c}^{i}_{ds,0}\,\mu^{i}_{0} + \bar{c}^{i}_{ds,1}\,\mu^{i}_{1})\right], \quad (32)$$

and

$$J^{T}_{ryr} = \sum_{i=1}^{M} \gamma^{i}_{ryr}\,(\mu^{i}_{1} - \bar{c}^{i}_{ds,0}\,\mu^{i}_{0} - \bar{c}^{i}_{ds,1}\,\mu^{i}_{1}). \quad (33)$$

Note that the average diadic subspace and junctional SR Ca^{2+} concentrations can also be written in terms of the moments,

$$c^{avg}_{ds} = E[\tilde{c}_{ds}] = \sum_{i=1}^{M} \pi^{i}E^{i}[\bar{c}^{i}_{ds,0} + \bar{c}^{i}_{ds,1}\,\tilde{c}_{jsr}] = \sum_{i=1}^{M}(\bar{c}^{i}_{ds,0}\,\mu^{i}_{0} + \bar{c}^{i}_{ds,1}\,\mu^{i}_{1}), \quad (34)$$

$$c^{avg}_{jsr} = E[\tilde{c}_{jsr}] = \sum_{i=1}^{M} \pi^{i}E^{i}[\tilde{c}_{jsr}] = \sum_{i=1}^{M} \mu^{i}_{1}, \quad (35)$$

and $J^{T}_{ef\,flux} = v^{T}_{ef\,flux}\left[c^{avg}_{ds} - c_{myo}\right]$ and $J^{T}_{refill} = v^{T}_{refill}[c_{nsr} - c^{avg}_{jsr}]$ when expressed in terms using these quantities.

Derivation of moment equations

Differentiating Eq. 28 with respect to time and using the equations of the univariate probability density approach (Eqs. 19–25), we obtain a system of ODEs that describe the time-evolution of these moments defined in Eq. 28,

$$\frac{d\mu_q^i}{dt} = \frac{q\mu_{q-1}^i}{\lambda_{jsr}^T}(v_{refill}^T c_{nsr} + \gamma_{ryr}^i v_{ryr}^T \bar{c}_{ds,0}^i) + \frac{q\mu_q^i}{\lambda_{jsr}^T}(\gamma_{ryr}^i v_{ryr}^T \bar{c}_{ds,1}^i - v_{refill}^T - \gamma_{ryr}^i v_{ryr}^T) + \sum_{j=1}^{M} \mu_q^j (K_\phi^{j,i} + \bar{c}_{ds,0}^j K_{ds}^{j,i}) + \sum_{j=1}^{M} \mu_{q+1}^j (\bar{c}_{ds,1}^j K_{ds}^{j,i} + K_{jsr}^{j,i}), \quad (36)$$

where $M = 12$, $1 \le i \le M$, $q = 0, 1, 2, \ldots$, and $\bar{c}_{ds,0}^j$ and $\bar{c}_{ds,1}^j$ are given by Eqs. 22 and 23. In this expression the CaRU model is specified by the $M \times M$ matrices K_ϕ, K_{ds}, and K_{jsr} defined in Eq. 17, and the superscripts in $K_\phi^{j,i}$, $K_{ds}^{j,i}$, and $K_{jsr}^{j,i}$ indicate the transition rate or bimolecular rate constant in the j^{th} row and i^{th} column of these matrices. Note that, in the M equations for the zeroth moments (μ_0^i), the first two terms evaluate to zero because $q = 0$. When $q \ge 1$, the first term depends on both the network SR [Ca^{2+}] (c_{nsr}) and the bulk myoplasmic [Ca^{2+}] (c_{myo}) through $\bar{c}_{ds,0}^j$. The terms in the first summation have a similar dependence on c_{myo} and this can affect transitions mediated by diadic subspace Ca^{2+} ($K_{ds}^{j,i}$), and the magnitude of these terms depends also on voltage through $K_\phi^{j,i}(V)$. Perhaps most importantly, the presence of diadic subspace and junction SR Ca^{2+}-mediated transitions in the CaRU model implies that $d\mu_q^j/dt$ is a function of $\mu_{q+1}^1, \mu_{q+1}^2, \ldots, \mu_{q+1}^M$ whenever $K_{ds}^{j,i}$ or $K_{jsr}^{j,i}$ is nonzero. That is, Eq. 36 is an open system of the form

$$\frac{d\mu_0^i}{dt} = f_0^i(\{\mu_0^i\}, \{\mu_1^i\}), \quad (37)$$

$$\frac{d\mu_q^i}{dt} = f_q^i(\{\mu_{q-1}^i\}, \{\mu_q^i\}, \{\mu_{q+1}^i\}) \quad q = 1, 2, 3, \ldots, \quad (38)$$

where we write $\{\mu_q^i\}$ as a shorthand for $\mu_q^1, \mu_q^2, \ldots, \mu_q^M$. Consequently, Eq. 36 is unusable in its current form, because to determine the time-evolution of the q^{th} moments one needs to know the value of the $(q+1)^{th}$ moments.

Moment closure

To utilize Eq. 36, we truncate the open system at the second moment ($q = 2$) and close the system of ODEs by assuming that the third moment can be expressed as an algebraic function ϕ of the lower moments $(\mu_0^i, \mu_1^i, \mu_2^i)$; that is,

$$\frac{d\mu_0^i}{dt} = f_0^i(\{\mu_0^i\}, \{\mu_1^i\}), \quad (39)$$

$$\frac{d\mu_1^i}{dt} = f_1^i(\{\mu_0^i\}, \{\mu_1^i\}, \{\mu_2^i\}), \quad (40)$$

$$\frac{d\mu_2^i}{dt} = f_2^i(\{\mu_1^i\}, \{\mu_2^i\}, \{\phi(\mu_0^i, \mu_1^i, \mu_2^i)\}). \quad (41)$$

The remainder of this section derives the required expression of the form $\mu_3^i = \phi(\mu_0^i, \mu_1^i, \mu_2^i)$ (Eqs. 48–53). This is accomplished by specifying the function ϕ in a manner that would be strictly correct if the probability density functions were scaled β-distributions. Note that choosing this form of ϕ to perform the moment closure given by Eqs. 39–41 is not equivalent to assuming that the probability density functions are well approximated by β-distributions. What we are assuming is that the relationship between μ_3^i and the lower moments $(\mu_0^i, \mu_1^i, \mu_2^i)$ is similar to the relationship observed in the β-distribution. This assumption is validated a posteriori by evaluating the accuracy of results obtained using this approach (see Figs. 2–6).

The derivation begins by considering a random variable $0 \le \tilde{x} \le 1$ that is functionally dependent on $\tilde{c}_{jsr}$ through

$$\tilde{x} = \frac{\tilde{c}_{jsr} - c_{jsr}^{min}}{\delta c_{jsr}} \quad \text{where} \quad \delta c_{jsr} = c_{jsr}^{max} - c_{jsr}^{min}. \quad (42)$$

In this expression, the minimum and maximum values of junctional SR [Ca^{2+}] are given by $c_{jsr}^{min} = \min_i \bar{c}_{jsr}^i$ and $c_{jsr}^{max} = \max_i \bar{c}_{jsr}^i$ where $\bar{c}_{jsr}^i$ are the steady-state values of c_{jsr} found by setting $f_{jsr}^i = 0$ in Eq. 20,

$$\bar{c}_{jsr}^i = \frac{\gamma_{ryr}^i v_{ryr}^T \bar{c}_{ds,0}^i + v_{refill}^T c_{nsr}}{v_{refill}^T + \gamma_{ryr}^i v_{ryr}^T (1 - \bar{c}_{ds,1}^i)},$$

where $\bar{c}_{ds,0}^i$ and $\bar{c}_{ds,1}^i$ are given by Eqs. 22 and 23. In this way, the maximum and minimum junctional SR Ca^{2+} concentrations are determined to be

$$c_{jsr}^{max} = c_{nsr} \quad (43)$$

$$c_{jsr}^{min} = \frac{v_*^T}{v_*^T + v_{refill}^T} c_{myo} + \frac{v_{refill}^T}{v_*^T + v_{refill}^T} c_{nsr}, \quad (44)$$

where $v_*^T = v_{ryr}^T v_{ef\,flux}^T / (v_{ryr}^T + v_{ef\,flux}^T)$. If the probability density for $\tilde{x}$ conditioned on CaRU state i were β-distributed, then

$$\Pr\{x < \tilde{x} < x + dx | \tilde{S} = i\} = \frac{x^{\alpha^i - 1}(1 - x)^{\beta^i - 1}\, dx}{B(\alpha^i, \beta^i)}, \quad (45)$$

where the β-function $B(\alpha^i, \beta^i)$ appears as a normalization constant and $\tilde{x}(t)$, $\tilde{S}(t)$, $\alpha^i(t)$, and $\beta^i(t)$ are all functions of time. Under this assumption, the first several conditional moments of $\tilde{x}$ would be

$$E^i[\tilde{x}] = \frac{\alpha^i}{\alpha^i + \beta^i}, \quad (46)$$

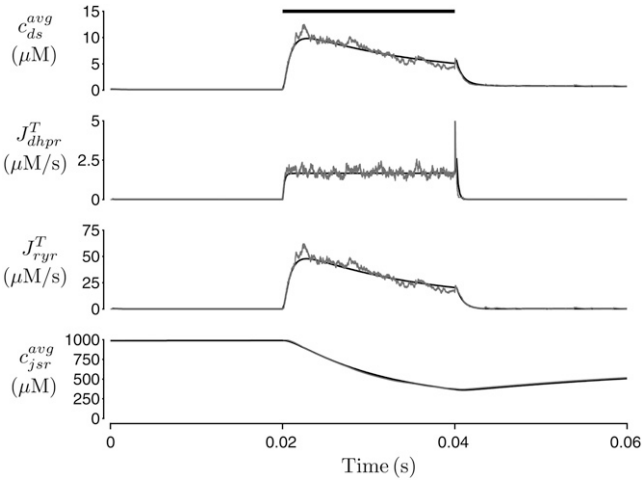

FIGURE 2 The response of the whole cell model during a 20-ms step depolarization from a holding potential of −80 mV to −10 mV (*bar*) with the Monte Carlo and moment-closure results indicated as a shaded line and solid line, respectively. (From *top* to *bottom*) Average diadic subspace $[Ca^{2+}]$ (c_{ds}^{avg}), total Ca^{2+} flux via the DHPR Ca^{2+} channels (J_{dhpr}^{T}), total Ca^{2+}-induced Ca^{2+} release flux (J_{ryr}^{T}), and average junctional SR $[Ca^{2+}]$ (c_{jsr}^{avg}). The Monte Carlo simulation used $N = 1000$ Ca^{2+} release units and parameters as in Tables 2–4.

$$E^{i}[\tilde{x}^2] = \frac{\alpha^{i}(\alpha^{i}+1)}{(\alpha^{i}+\beta^{i})(\alpha^{i}+\beta^{i}+1)}, \tag{47}$$

and inverting these expressions gives

$$\alpha^{i} = \frac{E^{i}[\tilde{x}](E^{i}[\tilde{x}] - E^{i}[\tilde{x}^2])}{E^{i}[\tilde{x}^2] - (E^{i}[\tilde{x}])^2}, \tag{48}$$

$$\beta^{i} = \alpha^{i}\left(\frac{1 - E^{i}[\tilde{x}]}{E^{i}[\tilde{x}]}\right). \tag{49}$$

Note that Eq. 42 implies the following relationship between the conditional moments of $\tilde{x}$ and $\tilde{c}_{jsr}$,

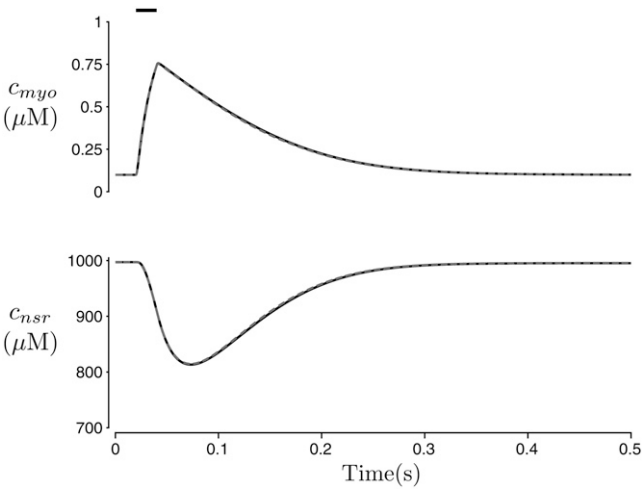

FIGURE 3 Solid lines show the dynamics of bulk myoplasmic (c_{myo}) and network SR (c_{nsr}) $[Ca^{2+}]$ in the whole-cell voltage-clamp protocol of Fig. 2 with step potential of −10 mV (note longer timescale). The dashed and solid lines are the Monte Carlo and moment-closure results, respectively.

$$E^{i}[\tilde{x}] = \frac{1}{\delta c_{jsr}}\left(\frac{\mu_1^{i}}{\mu_0^{i}} - c_{jsr}^{min}\right), \tag{50}$$

$$E^{i}[\tilde{x}^2] = \frac{1}{(\delta c_{jsr})^2}\left(\frac{\mu_2^{i}}{\mu_0^{i}} - 2c_{jsr}^{min}\frac{\mu_1^{i}}{\mu_0^{i}} + (c_{jsr}^{min})^2\right), \tag{51}$$

where we have used $\mu_q^{i} = \mu_0^{i}E^{i}[(c_{jsr})^q]$ for $q = 0$, 1, and 2; consequently, α^{i} and β^{i} can be found as a function of μ_0^{i}, μ_1^{i}, and μ_2^{i}. These parameters allow us to approximate the third conditional moment of $\tilde{x}$,

$$E^{i}[\tilde{x}^3] = \frac{\alpha^{i}(\alpha^{i}+1)(\alpha^{i}+2)}{(\alpha^{i}+\beta^{i})(\alpha^{i}+\beta^{i}+1)(\alpha^{i}+\beta^{i}+2)}, \tag{52}$$

which, in turn, allows us to approximate the third conditional moment of junctional SR $[Ca^{2+}]$ given by $\mu_3^{i} = \mu_0^{i}E^{i}[(\tilde{c}_{jsr})^3]$, where

$$\begin{aligned} E^{i}[(\tilde{c}_{jsr})^3] &= E^{i}\left[(\delta c_{jsr}\tilde{x} + c_{jsr}^{min})^3\right] \\ &= (\delta c_{jsr})^3E^{i}[\tilde{x}^3] + 3(\delta c_{jsr})^2c_{jsr}^{min}E^{i}[\tilde{x}^2] \\ &\quad - 3\delta c_{jsr}(c_{jsr}^{min})^2E^{i}[\tilde{x}] + (c_{jsr}^{min})^3. \end{aligned}$$

After some simplification one obtains

$$\mu_3^{i} = \mu_0^{i}(\delta c_{jsr})^3E^{i}[\tilde{x}^3] + 3c_{jsr}^{min}\mu_2^{i} - 3(c_{jsr}^{min})^2\mu_1^{i} + \mu_0^{i}(c_{jsr}^{min})^3, \tag{53}$$

which is an expression that takes the form $\mu_3^{i} = \phi(\mu_0^{i}, \mu_1^{i}, \mu_2^{i})$ as required by Eq. 41, because $E^{i}[\tilde{x}^3]$ is a function of μ_0^{i}, μ_1^{i}, and μ_2^{i} given by Eqs. 48–52.

Note that the expression $\mu_3^{i} = \phi(\mu_0^{i}, \mu_1^{i}, \mu_2^{i})$ derived above is one of several possibilities that we tested, but the only one that could be validated. For example, when ϕ was chosen in a manner that would be strictly correct if the probability densities were scaled normal or log-normal distributions, the resulting moment closure did not perform well (not shown). Using the β-distribution to derive ϕ makes sense because it is a continuous distribution defined on a finite interval. In addition, for particular values of α^{i} and β^{i}, the β-distribution (while remaining integrable) diverges at the boundaries ($\tilde{x} = 0$ or 1). Similarly, prior work has established that the densities $\rho^{i}(c_{jsr}, t)$ can accumulate probability at the minimum and maximum junctional SR Ca^{2+} concentrations (Eqs. 43 and 44) and diverge as $c_{jsr} \to c_{jsr}^{min}$ or c_{jsr}^{max} (18,22). As mentioned above, the use of the β-distribution to derive ϕ is ultimately validated by evaluating the accuracy of results obtained using this approach (see Figs. 2–6).

Representative Monte Carlo and moment-closure results

Fig. 2 shows representative results from the minimal whole cell model of EC coupling described above. In this simulated voltage-clamp protocol, the holding potential of −80 mV is

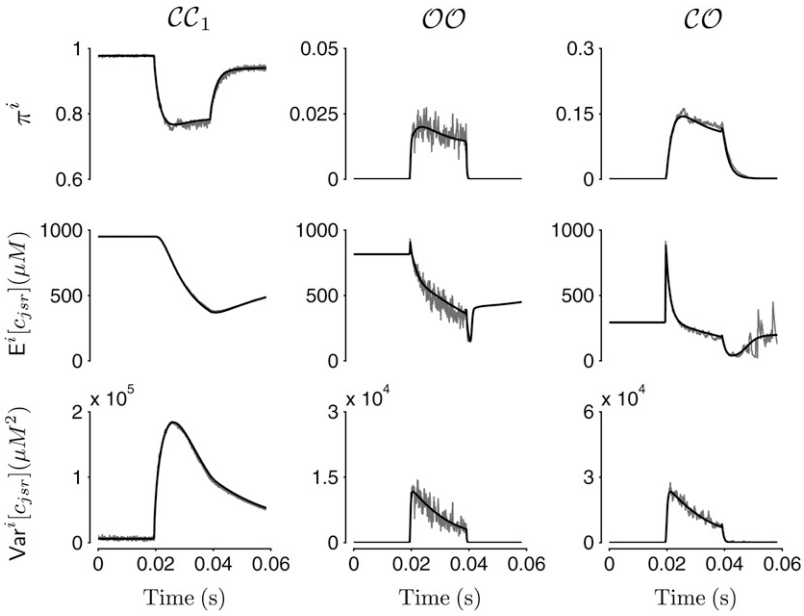

FIGURE 4 Comparison between results obtained from Monte Carlo (*shaded line*) simulations and moment-closure approach (*solid line*) for the probability (π^i), the conditional expectation of c_{jsr} ($E^i[\tilde{c}_{jsr}]$), and the conditional variance of c_{jsr} ($\mathrm{Var}^i[\tilde{c}_{jsr}]$), for three selected CaRU states, $\mathcal{CC}_1$ (*left column*), $\mathcal{OO}$ (*middle column*), and $\mathcal{CO}$ (*right column*). The Monte Carlo simulation used $N = 2000$ Ca^{2+} release units.

followed by a 20-ms duration test potential to −10 mV. The Monte Carlo result (*shaded line*) which involves a large but finite number of Ca^{2+} release units ($N = 1000$) can be easily spotted by the fluctuations due to the stochastic gating of the CaRUs. The moment-closure result (*solid line*) that assumes $N \to \infty$ lacks these fluctuations. The top and bottom panels of Fig. 2 show the average diadic subspace ($c_{ds}^{avg} = N^{-1}\sum_{n=1}^{N} c_{ds}^{n}$) and junctional SR ($c_{jsr}^{avg} = N^{-1}\sum_{n=1}^{N} c_{jsr}^{n}$) Ca^{2+} concentrations in the Monte Carlo calculation (*shaded lines*) as well as the corresponding quantities from the moment-closure calculation (*solid lines*, Eqs. 34 and 35). The middle two panels of Fig. 2 show the total Ca^{2+} influx through L-type Ca^{2+} channels ($J_{dhpr}^{T} = \sum_{n=1}^{N} J_{dhpr}^{n}$) and the total Ca^{2+} release from the RyR Ca^{2+} channels ($J_{ryr}^{T} = \sum_{n=1}^{N} J_{ryr}^{n}$) for the Monte Carlo calculation (*shaded lines*) as well as the corresponding quantities for the moment-closure result (*solid lines*, Eqs. 32 and 33). In both the Monte Carlo and moment-closure calculations, the test potential of −10 mV leads to 16× gain, here defined as the ratio $\bar{J}_{ryr}^{T}/\bar{J}_{dhpr}^{T}$, where the overbar indicates an average over the duration of the pulse.

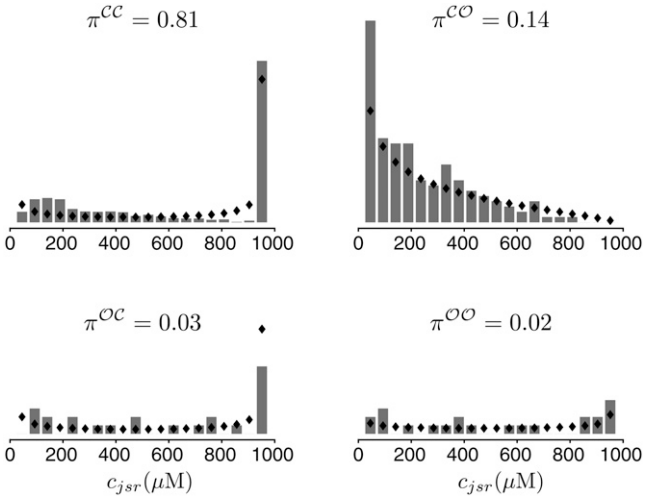

FIGURE 5 Histograms of junctional SR [Ca^{2+}] conditioned on CaRU state obtained by Monte Carlo simulation ($t = 30$ ms in Fig. 2). Solid diamonds show β-distributions with same mean and variance. Each panel corresponds to one of four agglomerated states of the CaRU: $\mathcal{CC}$, DHPR and RyR megachannel both closed; $\mathcal{OC}$, DHPR open and RyR megachannel closed; $\mathcal{CO}$, DHPR closed and RyR megachannel open; and $\mathcal{OO}$, DHPR and RyR megachannel both open.

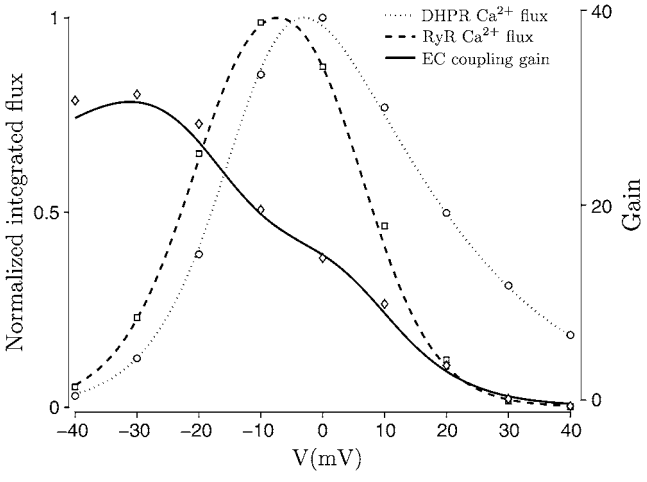

FIGURE 6 Summary of whole-cell voltage-clamp simulations such as those presented in Figs. 2–4 normalized to emphasize gradedness of Ca^{2+} release with respect to membrane potential and Ca^{2+} influx. Moment-closure results (*solid* and *broken lines*) agree with Monte Carlo calculations (*open symbols*) for a range of test potentials. Integrated Ca^{2+} influx via L-type channels ($\bar{J}_{dhpr}^{T}$) is shown as open circles (Monte Carlo) and dotted line (moment closure). Integrated RyR flux ($\bar{J}_{ryr}^{T}$) is shown as open squares (Monte Carlo) and dashed line (moment-closure). EC coupling gain ($\bar{J}_{ryr}^{T}/\bar{J}_{dhpr}^{T}$, *right axis*) is shown as open diamonds (Monte Carlo) and solid line (moment-closure).

Fig. 3 shows $[Ca^{2+}]$ in the bulk myoplasm (c_{myo}) and network SR (c_{nsr}) before, during, and after the -10 mV voltage pulse (note change in timescale). In both cases the moment-closure result is shown as a solid line while the Monte Carlo is displayed as a dashed line (note agreement). While junctional SR depletion develops rapidly after the initiation of the voltage pulse (not shown), refilling the junctional SR compartments via diffusion of Ca^{2+} from the network SR (J^{n}_{refill} in Eq. 2) depletes this compartment (c_{nsr}), which does not fully recover until ~300 ms after the termination of the voltage pulse.

Taken together, Figs. 2 and 3 validate our implementation of both the Monte Carlo and moment-closure approaches. Also note that the similarity of these results to Figs. 2 and 3 in Williams et al. (18) indicates that the six-state RyR megachannel model (Eq. 13)—used here because it takes the form of Eq. 17—has behavior similar to the two-state model of Williams et al. (18).

Dynamics of the moments of junctional SR $[Ca^{2+}]$

The top row of Fig. 4 shows the time evolution of the probability of three selected CaRU states during the simulated voltage-clamp protocol of Figs. 2 and 3, as calculated using both the Monte Carlo (*shaded lines*) and moment-closure (*solid lines*) methods. Before the voltage pulse, the probability of state $\mathcal{CC}_1$ (DHPR in state $\mathcal{C}$ and RyR in state $\mathcal{C}_1$, see Eqs. 13–16) is ~1, but during the voltage pulse to -10 mV this probability drops to ~0.78 (20–40 ms). Conversely, the probability of CaRU state $\mathcal{OO}$ (DHPR open and RyR open) and $\mathcal{CO}$ (DHPR closed and RyR open) both increase during the voltage pulse. The dynamics of voltage-dependent activation of DHPRs and subsequent triggering of the opening of RyR megachannels is similar in both the Monte Carlo (*shaded lines*) and moment-closure (*solid lines*) calculations.

The second row of Fig. 4 shows the mean junctional SR $[Ca^{2+}]$ conditioned on CaRU state for the Monte Carlo (*shaded line*) and the moment-closure (*solid line*) techniques. In the Monte Carlo calculation this conditional mean is given by

$$\langle c_{jsr}\rangle^{i}(t) = \frac{1}{N^{i}} \sum_{n\in n^{i}} c^{n}_{jsr}, \tag{54}$$

where $N^{i}(t)$ is the number of CaRUs in state i at time t and $n^{i}(t) = \{n : \tilde{S}^{n} = i\}$ so that the sum includes only those CaRUs in state i. The corresponding quantity in the moment-closure technique is the conditional expectation $E^{i}[c_{jsr}] = \mu^{i}_{1}/\mu^{i}_{0}$ (Eq. 29). Note that before the voltage pulse the expectation of SR $[Ca^{2+}]$ is ~1000 μM when conditioning on CaRU state $\mathcal{CC}_1$, 851 μM when conditioning on CaRU state $\mathcal{OO}$, and 306 μM when conditioning on CaRU state $\mathcal{CO}$. That is, at the holding potential of -80 mV, the stochastic gating of CaRUs leads to depletion of junctional SR $[Ca^{2+}]$ associated with release sites with open RyR megachannels (more pronounced in $\mathcal{CO}$ than $\mathcal{OO}$ because the former state is longer-lived). However, the probability of CaRU states $\mathcal{OO}$ and $\mathcal{CO}$ is very low at -80 mV and, consequently, the expectation of junctional SR $[Ca^{2+}]$ irrespective of CaRU state given by the weighted average

$$\langle c_{jsr}\rangle(t) = \frac{1}{N}\sum_{i=1}^{M} N^{i}\langle c_{jsr}\rangle^{i}$$

in the Monte Carlo model and

$$E[\tilde{c}_{jsr}] = \sum_{i=1}^{M} \pi^{i} E^{i}[\tilde{c}_{jsr}] = \sum_{i=1}^{M} \mu^{i}_{1}$$

in the moment-closure calculation is ~1000 μM, consistent with Fig. 2. Also note that during the voltage pulse the conditional expectation of junctional SR $[Ca^{2+}]$ decreases for CaRU states $\mathcal{CC}_1$ and $\mathcal{OO}$, but first increases and then decreases for CaRU state $\mathcal{CO}$, presumably because the increasing probability of state $\mathcal{CO}$ during the pulse is due to CaRU transitions into this state from others (such as $\mathcal{CC}_1$) that have higher resting junctional SR $[Ca^{2+}]$.

The third row of Fig. 4 shows the variance of the junctional SR $[Ca^{2+}]$ conditioned upon the CaRU state for the Monte Carlo (*shaded line*) and the moment-closure (*solid line*) techniques. For the Monte Carlo calculation

$$\langle (c^{n}_{jsr} - \langle c_{jsr}\rangle^{i})\rangle^{2>i} = \frac{1}{N^{i}}\sum_{n\in n^{i}} (c^{n}_{jsr} - \langle c_{jsr}\rangle^{i})^{2},$$

where N^{i} and $n^{i}(t)$ are defined as in Eq. 54, while the corresponding conditional variance of the junctional SR $[Ca^{2+}]$ in the moment-closure calculation is $Var^{i}[\tilde{c}_{jsr}] = \mu^{i}_{2}/\mu^{i}_{0} - (\mu^{i}_{1}/\mu^{i}_{0})^{2}$ (Eq. 30). Note that during the voltage pulse the conditional variance of c_{jsr} increases, as the dynamics of EC coupling lead to increased heterogeneity of junctional SR $[Ca^{2+}]$, and that the moment-closure technique accurately accounts for this heterogeneity (compare *shaded* and *solid lines*).

The distribution of junctional SR $[Ca^{2+}]$ conditioned on CaRU state

Fig. 5 shows a snapshot of the distribution of junctional SR $[Ca^{2+}]$ (c_{jsr}) conditioned upon the state of the Ca^{2+} release unit at $t = 30$ ms, midway through the voltage pulse protocol of Figs. 2–4. For clarity, the five closed states of the RyR megachannel ($\mathcal{C}_1, \mathcal{C}_2, \cdots, \mathcal{C}_5$ in Eq. 13) have been lumped resulting in a contracted presentation with four CaRU states: $\mathcal{CC}$, $\mathcal{CO}$, $\mathcal{OC}$, and $\mathcal{OO}$, where $\mathcal{CC} = \mathcal{CC}_1 \cdots \mathcal{CC}_5$ and $\mathcal{OC} = \mathcal{OC}_1 \cdots \mathcal{OC}_5$ (Eq. 16). Thus, the two histograms on the bottom of Fig. 5 indicate the distribution of JSR $[Ca^{2+}]$ when the DHPR is open ($\pi^{\mathcal{OC}} + \pi^{\mathcal{OO}} = 0.05$), while the two histograms on the right of Fig. 5 indicate the distribution of JSR $[Ca^{2+}]$ when the RyR megachannel is open ($\pi^{\mathcal{CO}} + \pi^{\mathcal{OO}} = 0.16$).

Fig. 5 shows a broad range of junctional SR $[Ca^{2+}]$ regardless of CaRU state, consistent with the high variances at $t = 30$ ms in Fig. 4. For example, when the RyR megachannel

is closed ($\mathcal{CC}$ and $\mathcal{OC}$, *left panels*), a randomly sampled junctional SR is likely to be replete, as indicated by the large vertical bar at $c_{jsr} \approx 1000\ \mu$M. However, one can also find depleted junctional SR [Ca^{2+}] associated with closed RyR megachannels, where RyRs have recently opened and the junctional SR has not had time to refill. Conversely, when the RyR is open ($\mathcal{CO}$ and $\mathcal{OO}$, *right panels*), the probability mass has shifted to lower junctional SR [Ca^{2+}].

The diamonds of Fig. 5 show β-distributions with the same mean and variance as the histograms obtained from Monte Carlo simulation. While the agreement is noteworthy, this correspondence is not required for the moment-closure technique to work well. What is required is that the relationship between the third (μ_3^i) and lower ($\mu_0^i, \mu_1^i, \mu_2^i$) moments in the histograms is similar to that observed in the β-distribution. For example, the histogram junctional SR [Ca^{2+}] for CaRU state $\mathcal{CO}$ at $t = 30$ ms has moments of $\mu_0^{\mathcal{CO}} = 0.14$, $\mu_1^{\mathcal{CO}} = 35.3\ \mu$M, $\mu_2^{\mathcal{CO}} = 1.59 \times 10^4 \mu\text{M}^2$, and $\mu_3^{\mathcal{CO}} = 9.17 \times 10^6 \mu\text{M}^3$. When moments 0–2 are used to estimate the third moment using Eq. 53 with $c_{jsr}^{min} = 22$ and $c_{jsr}^{max} = 981\ \mu$M (Eqs. 43 and 44), one obtains $\mu_3^{\mathcal{CO}} = 9.18 \times 10^6 \mu\text{M}^3$, for a relative error of only 0.1%. It is this low error that is responsible for the excellent agreement between the moment-closure result and the Monte Carlo calculation observed in Figs. 2–4.

The model displays gain and gradedness

To further validate the moment-closure approach by comparison to Monte Carlo simulation, Fig. 6 summarizes a large number of simulated whole-cell voltage-clamp protocols such as those presented in Figs. 2–4. The open circles of Fig. 6 show the trigger Ca^{2+} influx via L-type Ca^{2+} channels integrated over the 20-ms voltage step to test potentials in the range −40 to 40 mV using 1000 CaRUs (the plot is normalized to maximum value of $\bar{J}_{dhpr}^{T} = 0.038\ \mu$M). The dotted line of Fig. 6 shows that the trigger Ca^{2+} influx in the moment-closure calculation agrees with the Monte Carlo simulations. Similarly, the open squares of Fig. 6 show the voltage-dependence of the Ca^{2+} release flux (normalized to maximum value of $\bar{J}_{ryr}^{T} = 0.678\ \mu M$), while the dashed lines of Fig. 6 show that the Ca^{2+} release flux observed in the moment-closure calculation agrees with the Monte Carlo simulations. Note that the Monte Carlo and moment-closure calculations exhibit graded Ca^{2+} release. Furthermore, the EC coupling gain ($\bar{J}_{ryr}^{T}/\bar{J}_{dhpr}^{T}$) is a decreasing function of voltage, in the range of 32–15× for test potentials between −40 and 0 mV. Most importantly, the Monte Carlo and moment-closure calculations are nearly identical (compare *open diamonds* and *solid line*).

Computational efficiency of the moment-closure approach

While the previous sections have shown that the moment-closure and Monte Carlo calculations are essentially equivalent in terms of the dynamic cellular responses they predict, it is important to note that the moment-closure approach is significantly faster than Monte Carlo simulation. The Monte Carlo simulations presented above are performed using $\Delta t = 0.01\ \mu$s, a value chosen so the probability of transition occurring in each CaRU is <5% per time step. Table 1 shows that the run time for these 60-ms simulations increases approximately linearly with the number of CaRU units; for example, an $N = 10{,}000$ simulation takes ~11 times longer than a $N = 1000$ simulation. When our current implementation of the moment-closure method is employed using a nonadaptive time step of $\Delta t = 0.01\ \mu$s, the run time is 95 min, which is ~100 times faster than Monte Carlo simulations with a physiologically realistic number of CaRUs (e.g., $N = 10{,}000$). However, a time step of 0.01 μs is much smaller than required for integrating the moment-closure ODEs. When this artificial constraint is removed and the moment-closure approach is benchmarked using a nonadaptive time step as large as numerical stability will allow, the calculations are 8755:0.9 = 9728 times faster than Monte Carlo simulations containing $N = 10{,}000$ CaRUs. That is, the computational efficiency of the moment-closure approach is nearly four orders-of-magnitude superior to physiologically realistic Monte Carlo simulations, while leading to nearly identical results (see Figs. 2–4, and 6). Furthermore, integration methods that utilize adaptive time-stepping are likely to further enhance the computational advantage of the moment-closure approach to modeling local control of EC coupling.

Restitution of CICR studied using moment-closure approach

To show how the computational efficiency of the moment-closure approach facilitates studies that can provide biophysical insight, we present a study of the restitution of Ca^{2+}-induced Ca^{2+} release during simulated two-pulse voltage-clamp protocols (see (24)). As diagrammed in the inset, Fig. 7 *A* plots the ratio of the integrated release during the two pulses ($\bar{J}_{ryr}^{T(2)}/\bar{J}_{ryr}^{T(1)}$) as a function of time between the end of the first pulse and beginning of the second (denoted by τ). Using the standard value for the maximum reuptake flux ($v_{serca}^{T} = 8.6\ \mu\text{M}^{-1}\ \text{s}^{-1}$), the time constant for recovery of CICR is ~93 ms. Increasing or decreasing v_{serca}^{T} by 20% (*dashed* and

TABLE 1 Run times required for a 60-ms simulation such as that presented in Fig. 2 using both Monte Carlo and moment-closure approaches

	Δt (μs)	N	Time (min)
Monte Carlo	0.01	100	50
	0.01	1000	794
	0.01	10,000	8755
Moment closure	0.01	—	95
	1	—	0.9

TABLE 2 Model parameters: volume fractions, Ca^{2+} buffering, and exchange between restricted domains and the bulk, physical constants, and fixed ion concentrations

Parameter	Definition	Value
N	Number of diadic subspaces	50–20,000
V_{nsr}	Network SR volume	3.15×10^{-7} μL
V_{myo}	Myoplasmic volume	2.15×10^{-5} μL
$V_{ds}^{T} = NV_{ds}$	Total diadic subspace volume	2×10^{-8} μL
$V_{jsr}^{T} = NV_{jsr}$	Total junctional SR volume	2.45×10^{-8} μL
C_m	Capacitive membrane area	1.534×10^{-4} μF
β_{ds}	Subspace buffering factor	0.5
β_{jsr}	Junctional SR buffering factor	0.065
β_{nsr}	Network SR buffering factor	1.0
β_{myo}	Myoplasmic buffering factor	0.05
$v_{refill}^{T} = \lambda_{jsr}^{T}/\tau_{refill}$	Junctional SR refilling rate	0.018 s^{-1}
$v_{efflux}^{T} = \lambda_{ds}^{T}/\tau_{efflux}$	Diadic subspace efflux rate	5.2 s^{-1}
F	Faraday's constant	96,480 Coul mol^{-1}
R	Gas constant	8314 mJ mol^{-1} K^{-1}
T	Absolute temperature	310 K
c_{ext}	Extracellular Ca^{2+} concentration	1.8 mM
$[Na^+]_{ext}$	Extracellular Na^+ concentration	140 mM
$[Na^+]_{myo}$	Intracellular Na^+ concentration	10.2 mM

dotted lines) leads to a time constant for CICR recovery of 80 ms and 120 ms, respectively. This result is qualitatively consistent with the results of Szentesi et al. (24), and the hypothesis that restitution of calcium release depends primarily on refilling of local SR calcium stores (24–26). As in Fig. 2, the moment-closure approach was validated by comparison to Monte Carlo simulation using these alternate values of v_{serca}^{T} and an interpulse interval of $\tau = 20$ ms (not shown).

The solid symbols in the four panels of Fig. 7 *B* show that in each of these three cases the expected value of the junctional SR $[Ca^{2+}]$ at the beginning of the second pulse is an increasing function of the interpulse interval τ. Also shown are the distributions of junctional SR $[Ca^{2+}]$ consistent with the conditional expectations and variances observed in the moment-closure model at the time of the second pulse begins when $\tau = 0.02$, 0.06, 0.1, and 0.2 s. Note that the rightmost extent of these distributions indicates the network SR $[Ca^{2+}]$

TABLE 3 Ca^{2+} release unit parameters (L-type Ca^{2+} channel and RyR cluster)

Parameter	Definition	Value
$v_{ryr}^{T} = Nv_{ryr}$	Total RyR cluster release rate	0.9 s^{-1}
$P_{dhpr}^{T} = NP_{dhpr}$	Total DHPR permeability	3.5×10^{-5} cm s^{-1}
V_{dhpr}^{θ}	DHPR activation threshold	−10 mV
σ_{dhpr}	DHPR activation parameter	6.24 mV
$\bar{k}_{dhpr}^{+}$	Maximum rate of DHPR opening	556 s^{-1}
k_{dhpr}^{-}	Closing rate of DHPR opening	5000 s^{-1}
k_{dhpr}^{-}	Rate of DHPR closing	5000 s^{-1}
k_{ryr}^{+}	Rate of RyR activation	2000 $\mu M^{-1} s^{-1}$
k_{ryr}^{-}	Rate of RyR deactivation	1600 s^{-1}
$k_{ryr,*}^{+}$	Rate of RyR opening	40 $\mu M^{-1} s^{-1}$
$k_{ryr,*}^{-}$	Rate of RyR closing	500 s^{-1}
α	Cooperativity factor	2
β	Cooperativity factor	2

TABLE 4 Model parameters: Na^+-Ca^{2+} exchange current, SERCA pumps, and background Ca^{2+} influx

Parameter	Definition	Value
K_{fs}	Forward half-saturation constant for SERCA pump	0.17 μM
K_{rs}	Reverse half-saturation constant	1702 μM
η_{fs}	Forward cooperativity constant	0.75
η_{rs}	Reverse cooperativity constant	0.75
v_{serca}	Maximum SERCA pump rate	8.6 $\mu M\ s^{-1}$
I_{ncx}^{o}	Magnitude of Na^+-Ca^{2+} exchange current	150 $\mu A\ \mu F^{-1}$
$K_{ncx,\,n}$	Na^+ half-saturation constant	87.5×10^3 μM
$K_{ncx,\,c}$	Ca^{2+} half-saturation constant	1.38×10^3 μM
k_{ncx}^{sat}	Saturation factor	0.1
η_{ncx}	Voltage dependence of Na^+-Ca^{2+} exchange	0.35
v_{leak}	SR Ca^{2+} leak rate constant	2.4×10^{-6} s^{-1}
g_{in}	Maximum conductance of background Ca^{2+} influx	9.6×10^{-5} mS μF^{-1}

in the corresponding simulation ($c_{jsr} \leq c_{nsr}$), and the fully recovered distribution (*dotted lines*) has an expectation of ~1000 μM (*open triangle*). Note that the variance of the junctional SR $[Ca^{2+}]$ decreases as a function of the interpulse interval τ (compare widths of distributions).

Fig. 8 shows the recovery of the network SR $[Ca^{2+}]$ (*dotted line*), the junctional SR $[Ca^{2+}]$ (*solid line*), and the average concentration when the two compartments are aggregated according to their effective volumes (*dashed line*). This last measure represents the total SR content as would be assessed experimentally via the rapid application of caffeine. Importantly, the restitution of CICR as probed by the ratio of the integrated release ($\bar{J}_{ryr}^{T(2)}/\bar{J}_{ryr}^{T(1)}$, *solid circles*) is consistent with the recovery of the junctional SR $[Ca^{2+}]$, but not consistent with recovery of the network SR $[Ca^{2+}]$ or the aggregate concentration.

Fig. 9 *A* is similar to Fig. 7 *A* except that, in this case, the rate of calcium diffusion from network SR to junctional SR (v_{refill}^{T}) is modified from the standard value of $v_{refill}^{T} = 0.018$ $\mu M^{-1}\ s^{-1}$. Despite the fact that the restitution of CICR follows the recovery of junctional SR $[Ca^{2+}]$ (see Fig. 8), the time constant of CICR restitution is less sensitive to the junctional SR refill rate (v_{refill}^{T}) than the maximum SERCA pump rate (v_{serca}^{T}). For example, increasing or decreasing v_{refill}^{T} by a factor of 2 (*dashed* and *dotted lines*) leads to a time constant for CICR recovery of 91 and 105 ms (similar to the standard value of 93 ms). Conversely, the extent of junctional SR depletion at the end of the first pulse ranges from 51–65% in Fig. 9 *A* and 58–59% in Fig. 7, and thus appears to be more sensitive to the value of v_{refill}^{T} than v_{serca}^{T} (a range proportional to the parameter variation in Fig. 9 *A* in the former range would span 2.5 rather than 14%).

Consistent with these observations, Fig. 9 *B* shows that the expected value of junctional SR $[Ca^{2+}]$ increases with increasing interpulse interval τ and that decreased values of v_{refill}^{T} lead to increased depletion (compare *solid triangles*).

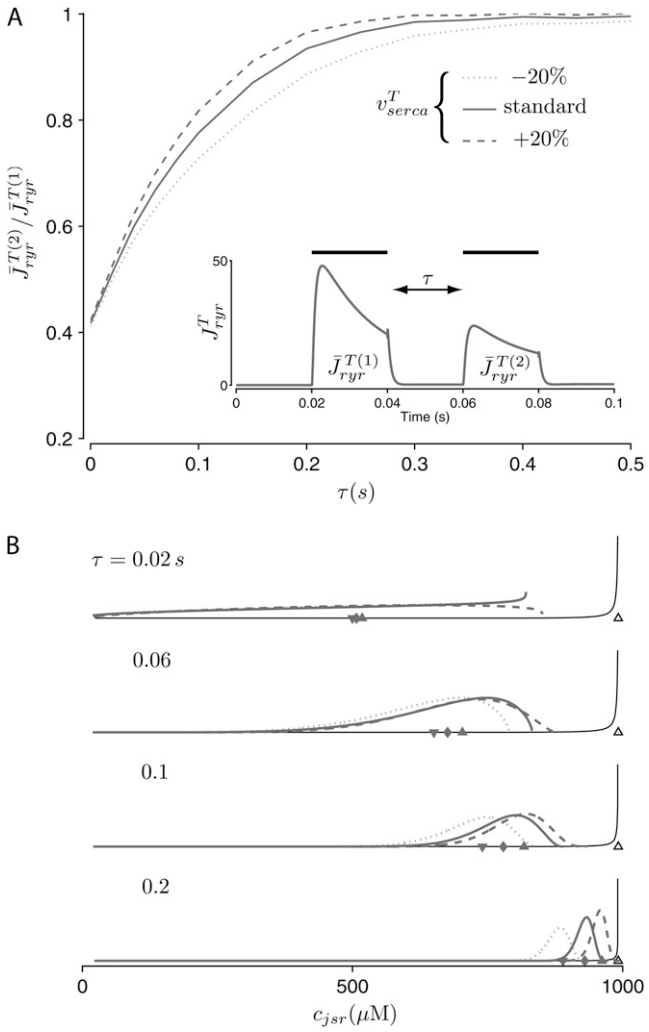

FIGURE 7 CICR restitution study using a simulated two-pulse voltage-clamp protocol and different values of the maximum reuptake flux $v^{\mathrm{T}}_{\mathrm{serca}}$. (*A*) Ratio of the integrated release during the two pulses ($\bar{J}^{\mathrm{T}(2)}_{\mathrm{ryr}}/\bar{J}^{\mathrm{T}(1)}_{\mathrm{ryr}}$) as a function of time between the end of the second pulse and beginning of the first (τ). Parameters: $v^{\mathrm{T}}_{\mathrm{serca}} = 6.88$ (*dotted line*), 8.60 (*solid line*), and 10.32 $\mu\mathrm{M}^{-1}\ \mathrm{s}^{-1}$ (*dashed line*), and as in Tables 2–4. (*Inset*) Timing of voltage pulses from –80 to −10 mV. (*B*) Distributions of junctional SR [Ca^{2+}] consistent with the conditional expectations and variances observed in the moment-closure model at the beginning of the second pulse when $\tau = 0.02$, 0.06, 0.1, and 0.2 s. Dotted, solid, and dashed lines indicate value of $v^{\mathrm{T}}_{\mathrm{serca}}$ as in panel *A*. Solid symbols indicate the expected value of junctional SR [Ca^{2+}] given by $\mathrm{E}[\bar{c}_{\mathrm{jsr}}] = \sum_{\mathrm{i}} \pi^{\mathrm{i}} \mathrm{E}^{\mathrm{i}}[\bar{c}_{\mathrm{jsr}}]$ and Eq. 29. The solid line and open triangles correspond to the initial (and fully recovered) distribution.

Comparison of the reconstructed distributions indicates that decreased $v^{\mathrm{T}}_{\mathrm{refill}}$ slows the recovery of junctional SR [Ca^{2+}] and leads to increased heterogeneity, i.e., higher variance in junctional SR [Ca^{2+}] (compare *dotted* and *solid lines*).

DISCUSSION

In previous work (18) we showed that the probability density approach to modeling local control of Ca^{2+} release in cardiac

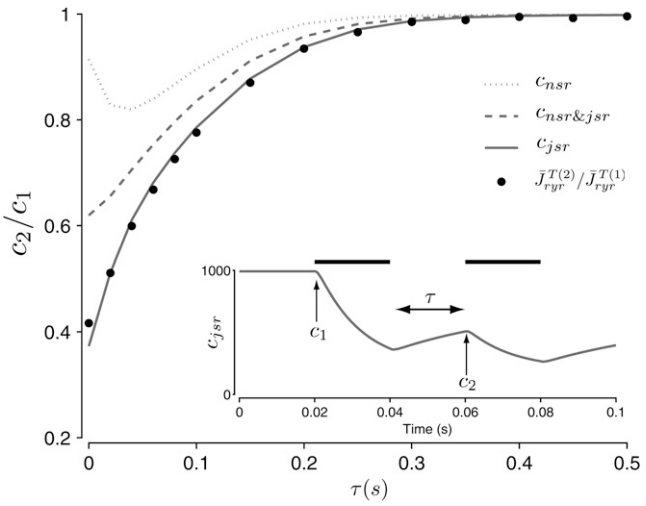

FIGURE 8 Recovery of the network SR [Ca^{2+}] (c_{jsr}, *dotted line*), the junctional SR [Ca^{2+}] (c_{nsr}, *solid line*), and the average concentration when the two compartments are aggregated according to their effective volumes ($c_{\mathrm{nsr\&jsr}}$, *dashed line*). (*Inset*) Timing of voltage pulses from −80 to −10 mV and representative c_{jsr} trace. Solid circles show CICR restitution observed in Fig. 7 *A*. Standard value of $v^{\mathrm{T}}_{\mathrm{serca}} = 8.60\ \mu\mathrm{M}^{-1}\ \mathrm{s}^{-1}$ used.

myocytes can be 30–650 times faster than traditional Monte Carlo simulations when the probability densities are univariate (i.e., functions of the junctional SR [Ca^{2+}] but not explicitly functions of diadic subspace [Ca^{2+}]). The derivation of the moment-closure technique presented in this article begins with a univariate probability density formulation, but the resulting simulations are nearly 10,000 times faster than Monte Carlo (see Table 1). For the whole-cell model that is the focus of this article, the moment-closure technique is thus significantly more efficient that our previously presented univariate probability density method (18).

Although the computational efficiency of the moment-closure technique in this local control context is exciting, it is important to note that the relative merits of Monte Carlo, probability density, and moment-closure methods are in general model-dependent. For example, the run time required for the Monte Carlo simulations such as Fig. 2 is, at least ultimately, an almost linear function of the number of CaRUs (see Table 1). Similarly, we have observed that the computational efficiency of the univariate probability density calculation presented in Williams et al. (18) scales linearly with the number of Ca^{2+} release unit states (M) and the number of mesh points used to discretize the junctional SR [Ca^{2+}]. Because the moment-closure approach results in $2 + 3M$ ODEs (bulk myoplasmic [Ca^{2+}], network SR [Ca^{2+}], and $\mu^{\mathrm{i}}_0, \mu^{\mathrm{i}}_1$, and μ^{i}_2 for each CaRU state), the computational demand of the moment-closure approach is expected to scale linearly with M. That is, increasing the number of CaRU states could reduce the computational advantage of the moment-closure approach relative to Monte Carlo.

While the CaRU model used here to introduce and validate the moment-closure approach includes a two-state DHPR

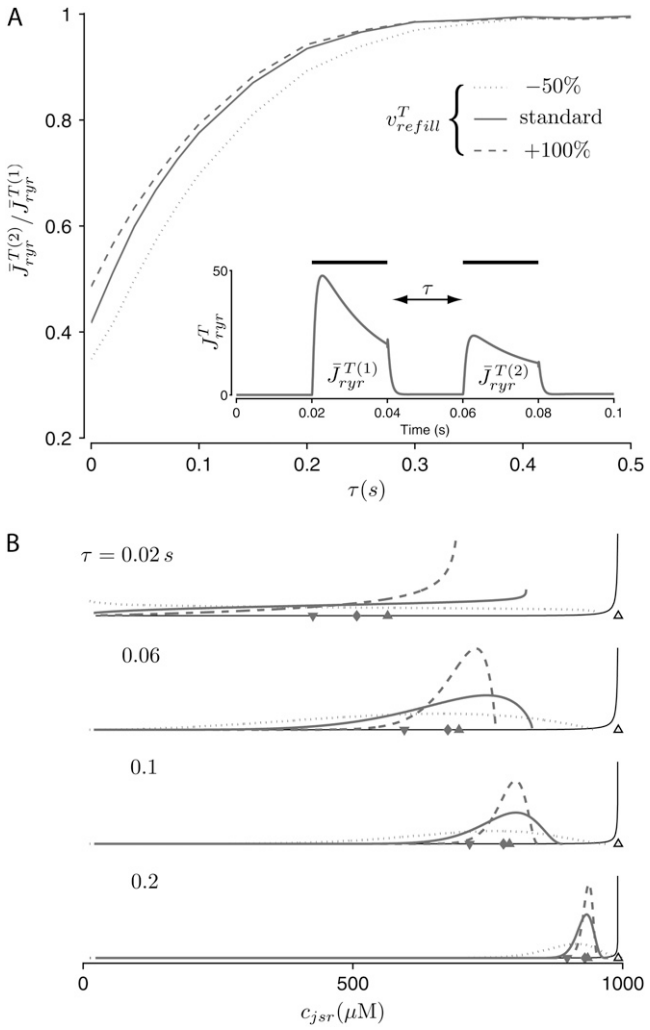

FIGURE 9 Summary of CICR restitution study using a simulated two-pulse voltage-clamp protocol and different values of the junctional SR refill rate given by $v^{\mathrm{T}}_{\mathrm{refill}} = 0.009$ (*dotted line*), 0.018 (*solid line*), and 0.036 $\mu\mathrm{M}^{-1}$ s^{-1} (*dashed line*). Standard value of $v^{\mathrm{T}}_{\mathrm{serca}} = 8.60$ $\mu\mathrm{M}^{-1}$ s^{-1} used. See legend to Fig. 7.

model and a six-state RyR megachannel (Eq. 16), the success of the moment equations (Eq. 36 and Eqs. 39–41) and moment-closure using $\mu^{\mathrm{i}}_3 = \phi(\mu^{\mathrm{i}}_0, \mu^{\mathrm{i}}_1, \mu^{\mathrm{i}}_2)$ given by Eqs. 48–53 does not depend on the CaRU model; rather, any CaRU that takes the form of Eq. 17 could be employed. For example, a more realistic DHPR model that includes voltage and Ca^{2+}-dependent inactivation would allow integration of the moment-closure approach to modeling local control of CICR and action potentials modeled using Hodgkin-Huxley-style membrane currents. Similarly, a more realistic CaRU model could be constructed as the composition of multiple RyR single channel models. This approach will therefore allow for the development of mechanistic, local control models that can examine phenomena such as stochastic SR calcium leak and bidirectional interactions between calcium transients and action potential morphology. However, to maintain the computational advantage of the moment-closure approach relative to Monte Carlo, the state-space explosion that inevitably occurs in compositional models is an important practical consideration. For example, one 12-state L-type channel and 12 four-state RyRs leads to a CaRU model with $M = 5460$ distinguishable states and thus >16,000 ODEs, a value approaching the 20,000 ODEs required in a 10,000 CaRU Monte Carlo simulation.

The moment-closure approach presented here begins with a univariate probability density approach to modeling heterogeneous junctional SR $[Ca^{2+}]$. This was motivated by our previous work in which we observed that model parameters lead to rapid equilibrium of the diadic subspace $[Ca^{2+}]$ with the $[Ca^{2+}]$ in the junctional SR and bulk myoplasm (18). When junctional SR $[Ca^{2+}]$ was also assumed to be rapidly equilibrated with the bulk myoplasmic and network SR Ca^{2+} concentrations so that these local Ca^{2+} concentrations could be expressed as algebraic functions of c_{myo}, c_{nsr}, and CaRU state (21,27), the resulting model did not exhibit high gain Ca^{2+} release that is graded with membrane potential (not shown). That is, the assumption that both diadic subspace $[Ca^{2+}]$ and junctional SR $[Ca^{2+}]$ are in quasi-static equilibrium with bulk myoplasmic and network SR Ca^{2+} leads to unacceptable errors and cannot be employed to accelerate this particular whole-cell model. This approximation has, however, been successfully employed in previous studies of cardiac CICR (21,27). It therefore seems likely that the model simplifications that can be employed depend on the details of both RyR gating and local concentration changes, issues that are currently being extensively studied.

In situations where rapid equilibration of diadic subspace $[Ca^{2+}]$ does not occur, the appropriate starting point for the moment-closure approach is a bivariate probability density model (18). While it is straightforward to derive the open system of ODEs analogous to Eq. 36 for the time-evolution of the moments of bivariate probability densities $\rho^{\mathrm{i}}(c_{\mathrm{ds}}, c_{\mathrm{jsr}}, t)$ defined by

$$\mu^{\mathrm{i}}_{\mathrm{p,q}}(t) = \int\int \rho^{\mathrm{i}}(c_{\mathrm{ds}}, c_{\mathrm{jsr}}, t)\,(c_{\mathrm{ds}})^{\mathrm{p}}\,(c_{\mathrm{jsr}})^{\mathrm{q}}\,dc_{\mathrm{ds}}\,dc_{\mathrm{jsr}},$$

we have yet to find a moment-closure method that works well in the bivariate case. This would be an important further development of the moment-closure approach as a computationally efficient alternative to Monte Carlo simulation of the local control of EC coupling in cardiac myocytes.

APPENDIX: WHOLE CELL MODEL OF EC COUPLING—FLUXES AND VOLUME RATIOS

The whole cell model of EC coupling that is the focus of this article includes several fluxes that directly influence the dynamics of the bulk myoplasmic and network SR $[Ca^{2+}]$. For example, the Na^+-Ca^{2+} exchanger current that appears in Eqs. 1 and 2 identical in the Monte Carlo, probability density, and moment-closure formulations and takes the form $J_{\mathrm{ncx}} = -A_{\mathrm{m}}I_{\mathrm{ncx}}/F$ where (2,10,28)

$$I_{\mathrm{ncx}} = I^{\mathrm{o}}_{\mathrm{ncx}} \frac{[\mathrm{Na}^+]^3_{\mathrm{myo}} c_{\mathrm{ext}} e^{\eta_{\mathrm{ncx}} \mathrm{FV/RT}} - [\mathrm{Na}^+]^3_{\mathrm{ext}} c_{\mathrm{myo}} e^{(\eta_{\mathrm{ncx}}-1)\mathrm{FV/RT}}}{(K^3_{\mathrm{ncx,n}} + [\mathrm{Na}^+]^3_{\mathrm{ext}})(K_{\mathrm{ncx,c}} + c_{\mathrm{ext}})(1 + k^{\mathrm{sat}}_{\mathrm{ncx}} e^{(\eta_{\mathrm{ncx}}-1)\mathrm{FV/RT}})}.$$

$A_{\mathrm{m}} = C_{\mathrm{m}}\beta_{\mathrm{myo}}/V_{\mathrm{myo}}$, c_{ext} is the extracellular Ca^{2+} concentration, and $[Na^+]_{\mathrm{myo}}$ and $[Na^+]_{\mathrm{ext}}$ are the intracellular and extracellular sodium concentrations, respectively (for parameters see (18)). The SERCA-type Ca-ATPase flux that appears in Eqs. 1 and 2 includes both forward and reverse modes (29) and is given by

$$J_{\mathrm{serca}} = v_{\mathrm{serca}} \frac{(c_{\mathrm{myo}}/K_{\mathrm{fs}})^{\eta_{\mathrm{fs}}} - (c_{\mathrm{nsr}}/K_{\mathrm{rs}})^{\eta_{\mathrm{rs}}}}{1 + (c_{\mathrm{myo}}/K_{\mathrm{fs}})^{\eta_{\mathrm{fs}}} + (c_{\mathrm{nsr}}/K_{\mathrm{rs}})^{\eta_{\mathrm{rs}}}},$$

with parameters as in Williams et al. (18). In addition, Eqs. 1 and 2 include a leakage Ca^{2+} flux given by

$$J_{\mathrm{leak}} = v_{\mathrm{leak}}(c_{\mathrm{nsr}} - c_{\mathrm{myo}}).$$

Following Rice et al. (28), Eq. 1 includes a constant background Ca^{2+} influx that takes the form $J_{\mathrm{in}} = -A_{\mathrm{m}} I_{\mathrm{in}}/zF$, where $I_{\mathrm{in}} = g_{\mathrm{in}}(V - E_{\mathrm{Ca}})$ and $E_{\mathrm{Ca}} = (RT/2F)\ln(c_{\mathrm{ext}}/c_{\mathrm{myo}})$.

The effective volume ratios λ_{nsr} and λ_{jsr} that appear in Eqs. 2 and 3 are defined with respect to the physical volume (V_{myo}) and include a constant-fraction Ca^{2+} buffer capacity for the myoplasm (β_{myo}). For example, the effective volume ratio associated with the network SR is

$$\lambda_{\mathrm{nsr}} = \frac{\hat{V}_{\mathrm{nsr}}}{\hat{V}_{\mathrm{myo}}} = \frac{V_{\mathrm{nsr}}/\beta_{\mathrm{nsr}}}{V_{\mathrm{myo}}/\beta_{\mathrm{myo}}},$$

with effective volumes defined by $\hat{V}_{\mathrm{nsr}} = V_{\mathrm{nsr}}/\beta_{\mathrm{nsr}}$ and $\hat{V}_{\mathrm{myo}} = V_{\mathrm{myo}}/\beta_{\mathrm{myo}}$. Because each individual junctional SR compartment is assumed to have the same physical volume (V_{jsr}) and buffering capacity (β_{jsr}), the effective volume ratio that occurs in Eq. 3 is

$$\lambda_{\mathrm{jsr}} = \frac{\hat{V}_{\mathrm{jsr}}}{\hat{V}_{\mathrm{myo}}} = \frac{V_{\mathrm{jsr}}/\beta_{\mathrm{jsr}}}{V_{\mathrm{myo}}/\beta_{\mathrm{myo}}} = \frac{1}{N}\left(\frac{V^{\mathrm{T}}_{\mathrm{jsr}}/\beta_{\mathrm{jsr}}}{V_{\mathrm{myo}}/\beta_{\mathrm{myo}}}\right), \qquad (55)$$

where the second expression defines λ_{jsr} in terms of the total physical volume of all the junctional SR compartments in aggregate ($V^{\mathrm{T}}_{\mathrm{jsr}} = NV_{\mathrm{jsr}}$). Similar assumptions and equations apply for the diadic subspaces so that the definition of λ_{ds} follows Eq. 55. However, when rapid equilibration of diadic subspace $[Ca^{2+}]$ is assumed, the volume ratio λ_{ds} no longer influences the steady state (see Eqs. 8–11 and Eqs. 21–23).

In the Monte Carlo model the trigger Ca^{2+} flux into each of the N diadic spaces through DHPR channels ($J^{\mathrm{n}}_{\mathrm{dhpr}}$ in Eq. 8) is given by

$$J^{\mathrm{n}}_{\mathrm{dhpr}} = -\frac{A_{\mathrm{m}}}{zF} I^{\mathrm{n}}_{\mathrm{dhpr}}, \qquad (56)$$

where $A_{\mathrm{m}} = C_{\mathrm{m}}\beta_{\mathrm{myo}}/V_{\mathrm{myo}}$. The inward Ca^{2+} current ($I^{\mathrm{n}}_{\mathrm{dhpr}} \le 0$) is given by

$$I^{\mathrm{n}}_{\mathrm{dhpr}} = \gamma^{\mathrm{n}}_{\mathrm{dhpr}} \frac{P^{\mathrm{T}}_{\mathrm{dhpr}}}{N}\left(\frac{zFV}{V_\theta}\right)\left(\frac{\bar{c}^{\mathrm{n}}_{\mathrm{ds}} e^{\mathrm{V/V}_\theta} - c_{\mathrm{ext}}}{e^{\mathrm{V/V}_\theta} - 1}\right), \qquad (57)$$

where $V_\theta = RT/zF$, $P^{\mathrm{T}}_{\mathrm{dhpr}}$ is the total (whole cell) permeability of the L-type Ca^{2+} channels, and $\gamma^{\mathrm{n}}_{\mathrm{dhpr}}$ is a random variable that is 0 when the L-type Ca^{2+} channel associated with the n^{th} CaRU is closed and 1 when this channel is open. Thus, the quantities $J^0_{\mathrm{dhpr}} = J^{\mathrm{T},0}_{\mathrm{dhpr}}/N$ and $J^1_{\mathrm{dhpr}} = J^{\mathrm{T},1}_{\mathrm{dhpr}}/N$ required to evaluate $\bar{c}^{\mathrm{n}}_{\mathrm{ds},0}$ (Eq. 10) and $\bar{c}^{\mathrm{n}}_{\mathrm{ds},1}$ (Eq. 11) are defined through

$$J^{\mathrm{T},0}_{\mathrm{dhpr}} = \frac{A_{\mathrm{m}} P^{\mathrm{T}}_{\mathrm{dhpr}} V}{V_\theta}\left(\frac{c_{\mathrm{ext}}}{e^{\mathrm{V/V}_\theta} - 1}\right)$$

$$J^{\mathrm{T},1}_{\mathrm{dhpr}} = \frac{A_{\mathrm{m}} P^{\mathrm{T}}_{\mathrm{dhpr}} V}{V_\theta}\left(\frac{e^{\mathrm{V/V}_\theta}}{1 - e^{\mathrm{V/V}_\theta}}\right),$$

consistent with Eq. 12. In the univariate probability density approach and moment-closure method the total flux through L-type Ca^{2+} channels is given by

$$J^{\mathrm{T}}_{\mathrm{dhpr}} = -A_{\mathrm{m}} P^{\mathrm{T}}_{\mathrm{dhpr}} \frac{V}{V_\theta}\left(\frac{\bar{c}^{\mathrm{n}}_{\mathrm{ds}} e^{\mathrm{V/V}_\theta} - c_{\mathrm{ext}}}{e^{\mathrm{V/V}_\theta} - 1}\right), \qquad (58)$$

and the quantities $J^{\mathrm{T},0}_{\mathrm{dhpr}}$ and $J^{\mathrm{T},1}_{\mathrm{dhpr}}$ are used to evaluate $\bar{c}^{\mathrm{i}}_{\mathrm{ds},0}$ (Eq. 22) and $\bar{c}^{\mathrm{i}}_{\mathrm{ds},1}$ (Eq. 23).

Note added in proof: When MATLAB's built-in stiff ordinary differential equation integrator ode15s is used rather than ode45, the moment-closure calculation can be accelerated by an additional factor of 20.

Some of these results have previously appeared in abstract form (30–32).

This material is based upon work supported by the National Science Foundation under grants No. 0133132 and 0443843. G.D.S. gratefully acknowledges a research leave during academic year 2007–2008 supported by the College of William and Mary and a long-term visitor position at the Mathematical Biosciences Institute at The Ohio State University.

REFERENCES

1. Cheng, H., W. Lederer, and M. Cannell. 1993. Calcium sparks: elementary events underlying excitation-contraction coupling in heart muscle. *Science*. 262:740–744.
2. Jafri, M., J. Rice, and R. Winslow. 1998. Cardiac Ca^{2+} dynamics: the roles of ryanodine receptor adaptation and sarcoplasmic reticulum load. *Biophys. J.* 74:1149–1168.
3. Glukhovsky, A., D. Adam, G. Amitzur, and S. Sideman. 1998. Mechanism of Ca^{2+} release from the sarcoplasmic reticulum: a computer model. *Ann. Biomed. Eng.* 26:213–229.
4. Snyder, S., B. Palmer, and R. Moore. 2000. A mathematical model of cardiocyte Ca^{2+} dynamics with a novel representation of sarcoplasmic reticular Ca^{2+} control. *Biophys. J.* 79:94–115.
5. Stern, M. 1992. Theory of excitation-contraction coupling in cardiac muscle. *Biophys. J.* 63:497–517.
6. Fabiato, A. 1985. Time and calcium dependence of activation and inactivation of calcium-induced release of calcium from the sarcoplasmic reticulum of a skinned canine cardiac Purkinje cell. *J. Gen. Physiol.* 85:247–289.
7. Wier, W., T. Egan, J. López-López, and C. Balke. 1994. Local control of excitation-contraction coupling in rat heart cells. *J. Physiol.* 474: 463–471.
8. Cannell, M., H. Cheng, and W. Lederer. 1995. The control of calcium release in heart muscle. *Science*. 268:1045–1049.
9. Bondarenko, V., G. Bett, and R. Rasmusson. 2004. A model of graded calcium release and L-type Ca^{2+} channel inactivation in cardiac muscle. *Am. J. Physiol. Heart Circ. Physiol.* 286:H1154–H1169.
10. Luo, C., and Y. Rudy. 1994. A dynamic model of the cardiac ventricular action potential. II. Afterdepolarizations, triggered activity, and potentiation. *Circ. Res.* 74:1097–1113.
11. Wong, A., A. Fabiato, and J. Bassingwaigthe. 1992. Model of calcium-induced calcium release in cardiac cells. *Bull. Math. Biol.* 54:95–116.
12. Hilgemann, D., and D. Noble. 1987. Excitation-contraction coupling and extracellular calcium transients in rabbit atrium: reconstruction of basic cellular mechanisms. *Proc. R. Soc. Lond. B. Biol. Sci.* 230: 163–205.
13. Shiferaw, Y., M. Watanabe, A. Garfinkel, J. Weiss, and A. Karma. 2003. Model of intracellular calcium cycling in ventricular myocytes. *Biophys. J.* 85:3666–3686.
14. Stern, M. D., L. S. Song, H. Cheng, J. S. Sham, H. T. Yang, K. R. Boheler, and E. Ríos. 1999. Local control models of cardiac excitation-contraction coupling. A possible role for allosteric interactions between ryanodine receptors. *J. Gen. Physiol.* 113:469–489.

15. Rice, J., M. Jafri, and R. Winslow. 1999. Modeling gain and gradedness of Ca^{2+} release in the functional unit of the cardiac diadic space. *Biophys. J.* 77:1871–1884.

16. Sobie, E., K. Dilly, J. dos Santos Cruz, W. Lederer, and M. Jafri. 2002. Termination of cardiac Ca^{2+} sparks: an investigative mathematical model of calcium-induced calcium release. *Biophys. J.* 83:59–78.

17. Greenstein, J., and R. Winslow. 2002. An integrative model of the cardiac ventricular myocyte incorporating local control of Ca^{2+} release. *Biophys. J.* 83:2918–2945.

18. Williams, G. S. B., M. A. Huertas, E. A. Sobie, M. S. Jafri, and G. D. Smith. 2007. A probability density approach to modeling local control of calcium-induced calcium release in cardiac myocytes. *Biophys. J.* 92:2311–2328.

19. Bers, D., and V. Stiffel. 1993. Ratio of ryanodine to dihydropyridine receptors in cardiac and skeletal muscle and implications for E-C coupling. *Am. J. Physiol.* 264:C1587–C1593.

20. Franzini-Armstrong, C. 1999. The sarcoplasmic reticulum and the control of muscle contraction. *FASEB J.* 13(Suppl 2):S266–S270.

21. Hinch, R. 2004. A mathematical analysis of the generation and termination of calcium sparks. *Biophys. J.* 86:1293–1307.

22. Mazzag, B., C. Tignanelli, and G. Smith. 2005. The effect of residual Ca^{2+} on the stochastic gating of Ca^{2+}-regulated Ca^{2+} channel models. *J. Theor. Biol.* 235:121–150.

23. Huertas, M., and G. Smith. 2007. The dynamics of luminal depletion and the stochastic gating of Ca^{2+}-activated Ca^{2+} channels and release sites. *J. Theor. Biol.* 246:332–354.

24. Szentesi, P., C. Pignier, M. Egger, E. Kranias, and E. Niggli. 2004. Sarcoplasmic reticulum Ca^{2+} refilling controls recovery from Ca^{2+}-induced Ca^{2+} release refractoriness in heart muscle. *Circ. Res.* 95: 807–813.

25. Terentyev, D., S. Viatchenko-Karpinski, H. H. Valdivia, A. L. Escobar, and S. Györke. 2002. Luminal Ca^{2+} controls termination and refractory behavior of Ca^{2+}-induced Ca^{2+} release in cardiac myocytes. *Circ. Res.* 91:414–420.

26. Sobie, E. A., L.-S. Song, and W. J. Lederer. 2005. Local recovery of Ca^{2+} release in rat ventricular myocytes. *J. Physiol.* 565:441–447.

27. Greenstein, J., R. Hinch, and R. Winslow. 2006. Mechanisms of excitation-contraction coupling in an integrative model of the cardiac ventricular myocyte. *Biophys. J.* 90:77–91.

28. Rice, J., M. Jafri, and R. Winslow. 2000. Modeling short-term interval-force relations in cardiac muscle. *Am. J. Physiol. Heart Circ. Physiol.* 278:H913–H931.

29. Shannon, T., K. Ginsburg, and D. Bers. 2000. Reverse mode of the sarcoplasmic reticulum calcium pump and load-dependent cytosolic calcium decline in voltage-clamped cardiac ventricular myocytes. *Biophys. J.* 78:322–333.

30. Williams, G., M. Huertas, E. Sobie, M. Jafri, and G. Smith. 2006. A probability density model of stochastic functional unit activity in cardiac myocytes. Biophysical Society Annual Meeting. 1079-Pos.

31. Williams, G., M. Huertas, E. Sobie, M. Jafri, and G. Smith. 2007. A probability density approach to modeling local control of calcium signaling in cardiac myocytes. Biophysical Society Annual Meeting. 1212-Pos.

32. Huertas, M., G. Williams, E. Sobie, M. Jafri, and G. Smith. 2008. A moment closure approach to modeling local control of calcium-induced calcium release in cardiac myocytes. Biophysical Society Annual Meeting. 494-Pos.

33. Huertas, M., G. Williams, and G. Smith. 2007. Moment closure approximations for a new class of whole cell models of Ca^{2+} handling representing heterogeneous domain Ca^{2+} concentrations. Biophysical Society Annual Meeting. 1210-Pos.